Thickness Determinations of the Lunar Surface Layer from Lunar Impact Craters

WILLIAM L. QUAIDE AND VERNE R. OBERBECK

Ames Research Center, Moffett Field, California 94035

Small, fresh lunar craters with normal, central-mound, flat-bottomed, and concentric geometry are widespread on maria surfaces. The same types of craters have been produced in the laboratory by impacting projectiles against targets consisting of loose, granular, noncohesive materials overlying cohesive substrates. The mechanics of formation of each laboratory crater type is described, and evidence is offered that the corresponding types of lunar craters are of impact origin. Extensive studies of the effects of lunar impact variables on the conditions of formation of these crater types show that a previously described statistical method can be used to determine the thickness of the lunar surfaces layer within narrow limits. Two independent methods for determining the layer thickness at specific points are presented. Thickness estimates of the Surveyor 1 site obtained previously from study of medium-resolution Orbiter 1 photographs are re-evaluated by using subsequently obtained high-resolution photographs, and thickness determinations of two additional areas are presented. The different areas examined have different surface layer thickness. The fragments of the surface are certainly partly of impact origin, but volcanic contributions may also be present. The maria substrates are probably composed of volcanic flow rocks with interbeds of fragmental material.

INTRODUCTION

Luna and Surveyor missions have shown that posits of fine-grained materials are widespread the lunar surface [*Gault et al.*, 1966; nnilson *et al.*, 1966; *Shoemaker et al.*, 1967; ott *et al.*, 1967; *Christensen et al.*, 1967; erkasov *et al.*, 1968]. Numerous physical perties have been measured, and all refered studies indicate that the material can be racterized most simply as a very slightly esive, fine-grained aggregate. *Rennilson et al.* 66] and later *Shoemaker et al.* [1967] recized that the fine-grained surface materials e of limited thickness in areas adjacent to Surveyor 1 and 3 spacecrafts. They noted t the blocks on the rims of small craters were greater in size than the blocks strewn about surface but that large craters contained cks in their ejecta aprons many times larger n blocks in the surrounding terrains. They umed that the larger blocks were derived m hard rocks beneath the fine-grained sure layer and placed limits on the thickness of layer by estimating the depths of the small craters containing such blocks.

hortly thereafter *Oberbeck and Quaide* 67], using Lunar Orbiter 1 photographs, esti- ed the distribution of thickness of the surface layer over 3000 km² of Oceanus Procellarum. They showed that fresh craters with diameters less than 250 meters display various but distinct morphologies with respect to their size and that this relationship could be interpreted on the basis of laboratory impact experiments. They impacted projectiles against targets with surficial granular layers of varying thickness overlying substrates of greater strength and produced the morphologic types of craters recognized on the moon. Photographs of these lunar crater types and their laboratory counterparts are shown in Figure 1. Boundary values separating realms of crater morphology for the laboratory craters were defined in terms of ratios of apparent crater diameter to surficial layer thickness. Because the boundary values appeared to be independent of velocity and angle of impact and strength of the cohesive substrate and because there was a regular relationship between size and crater morphology on the moon, it was reasonable to assume that the corresponding morphologic types of lunar craters could have originated by the impact process. Accordingly, the experimental boundary values were used to determine the thickness distribution of the surface layer in Oceanus Procellarum. However, their study of the effect of impact variables on the conditions of forma-

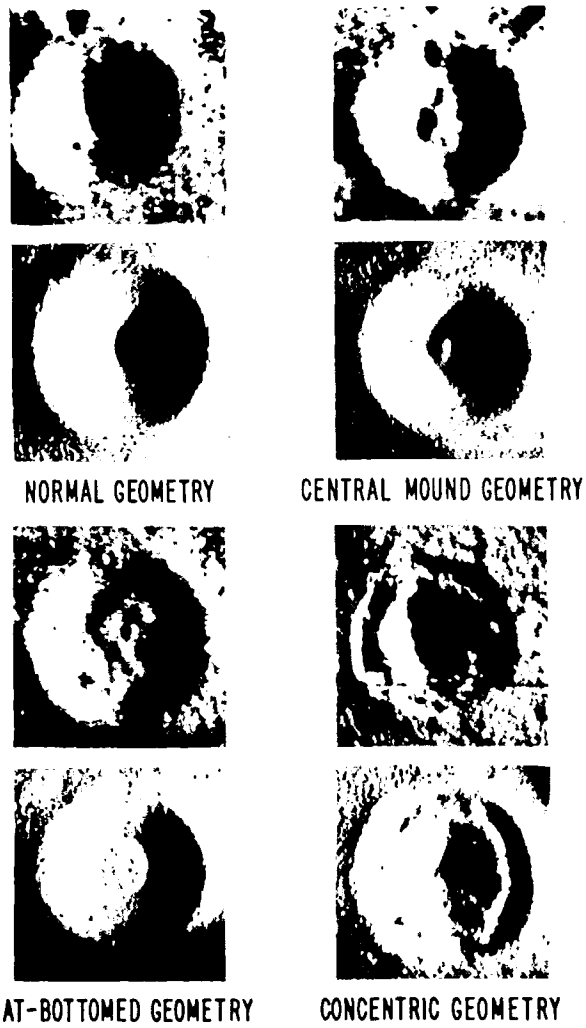

Fig. 1. Lunar craters with normal, central-mound, flat-bottomed, and concentric geometry and their laboratory counterparts.

tion of each morphologic type of crater was only rudimentary. The study of the influence of any one of the variables considered was not exhaustive, nor were all important variables considered.

This paper examines thoroughly the effects of significant lunar impact variables on the conditions of formation of each crater type, tests the hypothesis that these small lunar craters were formed by impact, and defines and applies techniques for measurement of the surface layer thickness.

Effects of Variables

The very regular relationship between morphology and size of lunar craters reported by *Oberbeck and Quaide* [1967] suggests that, if the craters were formed by impact, the conditions of formation of each type must have little dependence on the common lunar impact variables. This suggestion was partially confirmed by their preliminary study of the effect of angle and velocity of impact and strength of the substrate on the conditions of formation of these crater types. Their study of the effects of variables was neither exhaustive nor complete, however, and it is now necessary to consider thoroughly the effects of variations in velocity and angle of impact, projectile properties, angle of repose of surficial materials and strength of the substrate. Since experiments are most conveniently performed at earth gravity conditions, it is further necessary to compare the formation of these craters in earth gravity with formation in simulated lunar gravity fields.

The effects of these variables have been examined in two ways. Ratios of apparent crater diameter to surficial layer thickness, D_A/t, have been used to define boundaries separating realms of crater morphology and to calculate the distribution of thickness of the lunar surface layer [*Oberbeck and Quaide*, 1967]. It is useful, therefore, to determine the effects of the variables on the values of these boundary ratios. In addition, for flat-bottomed and concentric craters, the ratio of the diameter of the floor of the surficial crater to the apparent crater diameter, D_F/D_A, is used extensively because both values can be measured on lunar photographs and in the laboratory and because the ratio is sensitive to slight changes in the ratio D_A/t. It is therefore useful to consider D_F/D_A as a function of D_A/t for various conditions of impact.

These and other symbolic notations are used repeatedly in this study. They are listed below for ease of reference.

- a, height of the mound in a central-mound crater.
- D_A, apparent crater diameter (rim crest to rim crest).
- D_F, diameter of the floor of the surficial crater in flat-bottomed and concentric craters.
- D_I, apparent diameter of the inner crater in a concentric crater.
- D_{MP}, midpoint of diameter class interval.
- g, gravity field.
- h, apparent crater depth (rim crest to floor) of central-mound, flat-bottomed, and concentric craters.
- k, experim
  crater
  ground
  diamete
- KE_P, kinetic
- Md, mass di
- n, number
  phology
- N, number
  phologic
- t, surficial
- α, angle o
- γ, illumina
- μ, microns.

The variables stu
ditions of each s
gether with refere
are shown.

Strength of the
the most pronou
the boundaries se
phology. Results
presented first an
ence for examinin

T

Variable Studied	Su Li
Substrate strength	24-mes quartz 31° an repose
Impact velocity	24-mes quartz 31° an of repo
Impact angle	24-mesl quartz 31° an of repo
Projectile properties	24-mesl quartz 31° ang of repos
Angle of repose surficial materials	24-mesl quartz 6- to 8- 40° cru quartz
Gravity field	24-mesh quartz 31° angl of repos

k, experimental constant relating true crater diameter (diameter at original ground surface) to apparent crater diameter.
E_P, kinetic energy of the projectile.
Md, mass displaced.
n, number of craters of a particular morphology in a diameter class interval.
N, number of fresh craters of all morphologies in a diameter class interval.
t, surficial layer thickness.
α, angle of repose of surficial material.
γ, illumination angle.
μ, microns.

variables studied and the experimental conons of each study are listed in Table 1 toer with references to figures in which results shown.

trength of the substrate was found to have -most pronounced effect on the position of boundaries separating realms of crater morlogy. Results of this study are therefore ented first and used as a standard of refer for examining the effects of all other variables. Targets with substrates of 24-mesh quartz sand (70% by volume 0.5–1 mm, 30% < 0.5 mm) bonded by epoxy resin to unconfined compressive strengths of 1.4 bars ±30% and 68.5 bars ±5% were impacted at constant angle and velocity with the same projectile type. The results are shown in Figure 2, where ratios of D_F/D_A are plotted as a function of D_A/t. Best-fit curves are drawn through the plotted values for the 68.5-bar and the 1.4-bar substrate cases to illustrate the observed variations. In addition, bar graphs indicating the realms of crater morphology in terms of the ratio D_A/t for each substrate are shown. The variability of values of D_F/D_A as a function of D_A/t is negligible for the two substrate cases, as can be seen from the curves, nor is the position of the boundary separating realms of normal from central-mound and flat-bottomed geometry affected. There is a notable difference, however, in the position of the boundaries separating realms of flat-bottomed from concentric geometry for the two cases. Flat-bottom craters were observed to form over the stronger substrate up to a maximum

TABLE 1. Impact Variables Studied and Experimental Conditions of Each Study

iable idied	Surficial Layer	Substrate Material, Unconfined Compressive Strength	Impact Angle (from Horizontal)	Impact Velocity, km/sec	Projectile	Gravity Field	Air Pressure, μ	Results in Figure
rate ngth	24-mesh quartz sand, 31° angle of repose	1.4 bars ±30% 68.5 bars ±5%	90°	1	7.65×4.00mm Lexan cylinders	1 g	100	2
et ocity	24-mesh quartz sand, 31° angle of repose	68.5 bars ±5%	90°	1–7	7.65×4.00mm Lexan cylinders	1 g	100	3
et	24-mesh quartz sand, 31° angle of repose	1.4 bars ±30%	30° 45° 90°	1	7.65×4.00mm Lexan cylinders	1 g	100	4
etile perties	24-mesh quartz sand, 31° angle of repose	1.4 bars ±30%	45°	5–7	6.3mm spheres of Pyrex glass aluminum 7.65×4.00mm Lexan cylinders	1 g	100	5
of e ficial terials	24-mesh, 31° quartz sand; 6- to 8-mesh, 40° crushed quartz	68.5 bars ±5%	90°	1	7.65×4.00mm Lexan cylinders	1 g	100	6
ity d	24-mesh quartz sand, 31° angle of repose	1.4 bars ±30%	90°	1	7.65×4.00mm Lexan cylinders	1 g ⅛ g	100	7

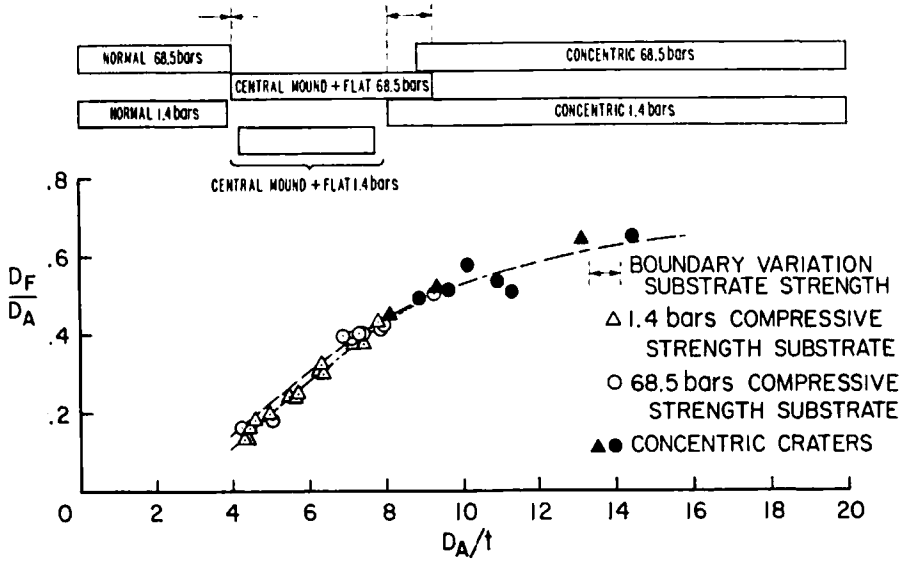

Fig. 2. Relationships between crater geometry and ratios of D_A/t and between ratios of D_F/D_A and D_A/t for craters produced in targets with substrates with unconfined compressive strength of 1.4 bars ± 30% and 68.5 bars ± 5%.

value of the ratio $D_A/t = 9.2$, and concentric craters were formed over the weaker substrates with values of D_A/t as low as 8.05. Thus, the maximum variation in position of the boundary separating realms of flat-bottomed from concentric geometry for these experimental conditions ranges from $D_A/t = 8$ to $D_A/t = 9.2$.

Variations in the velocity of impact from 1 to 7 km/sec have little effect on the relationship between the ratios D_F/D_A and D_A/t, as shown in Figure 3. There appears to be a slight deviation of the plotted points from the reference curves, but the agreement is generally g
There is no effect on the position of the bou
ary separating realms of normal from cen
mound and flat-bottomed geometry, but t
data indicate that there is a possible velo
dependence of the position of the bound
separating realms of flat-bottomed from
centric geometry. The largest value of D_A/t
flat-bottomed craters produced by hypervelo
impact against these targets was 9.25, essent
the same value as for the low-velocity case,
the smallest value of D_A/t observed for

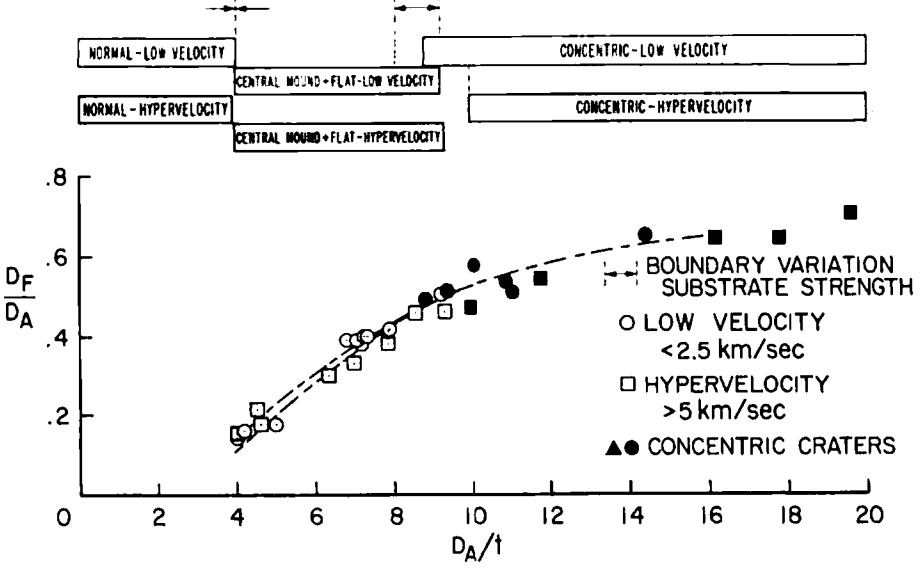

Fig. 3. Relationships between crater geometry and ratios of D_A/t and between ratios of D_F/D_A and D_A/t for craters produced by projectiles with velocities from 1 to 7 km/sec.

centric craters
define a range o
range of uncert
$D_A/t = 9.95$. Oth
in this study sug
experimental unc
variability proba
variability obtain
substrate strengt
The independe
formation of eac
ure 4. There are
between ratios of
angle, as indicate
about the refere
apparent systema
the boundaries se
phology. The bo
normal from cen
geometry is not
not appear to be
The position of t
bottomed from c
appears to be les
than by strength
range of variabilit
$D_A/t = 8$ to $D_A/$
by projectiles im
90°. The range o
the variability of

Fig. 4. Rela
D_F/D_A and D_A
the horizontal.

ric craters was 9.95. These data do not ne a range of variation but rather define a ge of uncertainty from $D_A/t = 9.2$ to $/t = 9.95$. Other hypervelocity data collected his study suggest, however, that this is an erimental uncertainty and that the range of iability probably lies within the range of iability obtained in the study of the effect of trate strength.

he independence of angle of impact on the nation of each crater type is shown in Fig- 4. There are no changes in the relationship ween ratios of D_F/D_A and D_A/t with impact le, as indicated by the clustering of points ut the reference curves, nor is there any arent systematic variation in the position of boundaries separating realms of crater mor- logy. The boundary separating realms of mal from central-mound and flat-bottomed metry is not precisely defined, but it does appear to be affected by angle of impact. position of the boundary separating flat- omed from concentric geometry, likewise, ears to be less affected by angle of impact by strength of substrate. The greatest e of variability shown by the data is from $/t = 8$ to $D_A/t = 8.5$ for craters produced projectiles impacting at angles of 45° and The range of experimental uncertainty of variability of position of the boundary for all angles of impact is from $D_A/t = 7.7$ to $D_A/t = 8.7$.

Effects of projectile properties were tested by varying the type of projectile while keeping all other conditions constant. Craters were produced by impacting 6.3-mm spherical projectiles of aluminum and Pyrex glass and 7.65 × 4.00 mm cylinders of Lexan against similar targets. Results of these tests are shown in Figure 5. The relationships between ratios of D_F/D_A and D_A/t are in perfect agreement with the reference curves. No data were obtained on the position of the boundary separating normal from central-mound and flat-bottomed geometry, nor is the evidence for effect on the position of the boundary separating flat-bottomed from concentric geometry extensive. Data from craters produced from aluminum projectiles indicate, however, that the range of uncertainty of this boundary position is within the range of variability defined on the basis of substrate strength variation.

During this study photographic records revealed that flat-bottomed and concentric craters undergo gravitational adjustment following the ejection process through collapse of initially steep crater walls to the angle of repose of the surficial materials. It is therefore obvious that the angle of repose of the material of the surface layer will influence D_F/D_A ratios of the flat-

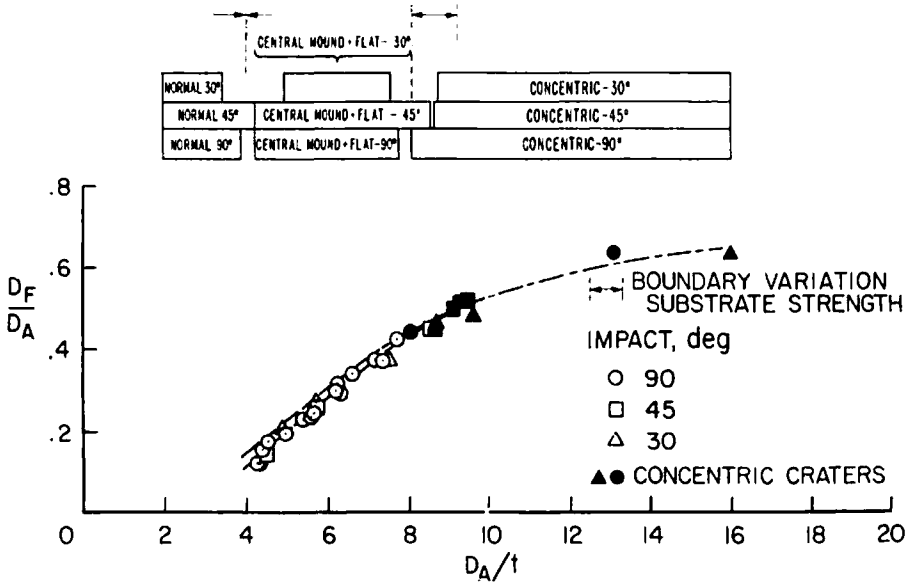

Fig. 4. Relationships between crater geometry and ratios of D_A/t and between ratios of D_F/D_A and D_A/t for craters produced by projectiles impacting at angles of 30° to 90° from the horizontal.

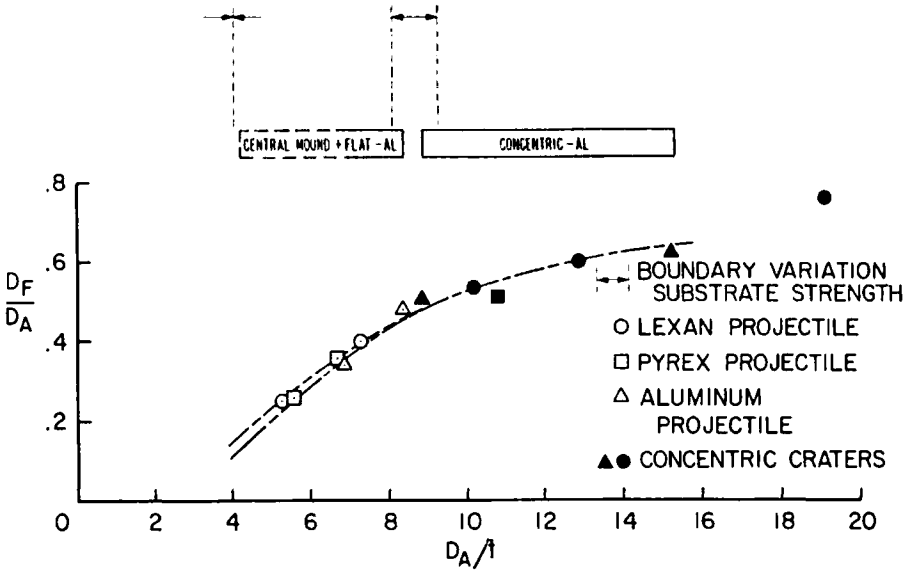

Fig. 5. Relationship between D_F/D_A and D_A/t for craters produced by 6.3-mm diameter spheres of aluminum and Pyrex and 7.65 × 4.00-mm cylindrical slugs of Lexan.

bottomed and concentric craters. The effect of angle of repose was investigated by impacting targets with two different surficial materials, 24-mesh quartz sand and 6- to 8-mesh angular crushed quartz with angles of repose of 31° and 40°, respectively. The results of the test indicate that the average slope angles of the crater walls, 30° and 38°, respectively, are determined by the angle of repose. D_F/D_A ratios can be calculated from the relationship:

$$D_F/D_A = k - (D_A/t)^{-1}2 \cot \alpha$$

where k is an experimental constant relating true diameter to apparent diameter for each surficial material, t is the surficial layer thickness, and α is the angle of repose of the surficial material. A comparison of predicted and observed ratios of D_F/D_A plotted as a function of ratios of D_A/t for targets consisting of 24-mesh quartz sand with an angle of repose of 31° and $k = 0.86$ and 6- to 8-mesh crushed quartz with an angle of repose of 40° and $K = 0.84$ are shown in Figure 6. The agreement is excellent for the 31° angle of repose material, but best fit for the 6- to 8-mesh crushed quartz data could be obtained only by using 38° as the angle of repose rather than the measured value of 40°. The boundaries separating realms of crater morphology do not appear to be affected significantly by angle of repose of the surficial materials studied. The boundary separating realms of normal from central-mound and flat-bottomed morphology was observed to occur at a slightly lower value of D_A/t than for the reference case, 3.8 compared with 4.05, but the flat-concentric boundary appears to be unaffected. The range of experimental uncertainty of this boundary position, from $D_A/t = 7.8$ to $D_A/t = 8.85$, very nearly corresponds to the range of variability determined from study of effects of strength variations. Thus, angle of repose has no significant effect on position of boundary values separating realms of crater morphology, but it does have a pronounced effect on relationships between D_F/D_A and D_A. However, the angle of repose of the lunar surface materials was estimated by measuring the interior slope angles of fresh flat-bottomed lunar craters, assuming that these craters form in a manner identical to that of laboratory flat-bottomed craters. The angle of repose so estimated for lunar surface material is 31° ± 2°. This value is in agreement with the estimate of *Choate* [1966], who reported angles of repose ranging from 33° to 35°. Accordingly, 24-mesh quartz sand with an angle of repose of 31° is acceptable as a model of the lunar surface material in the laboratory studies, and relationships between D_F/D_A and D_A/t so determined can be used with confidence.

Effects of the gravity field are more difficult to evaluate. Craters can be produced experimentally in a wide range of gravity fields by impacting projectiles against targets falling

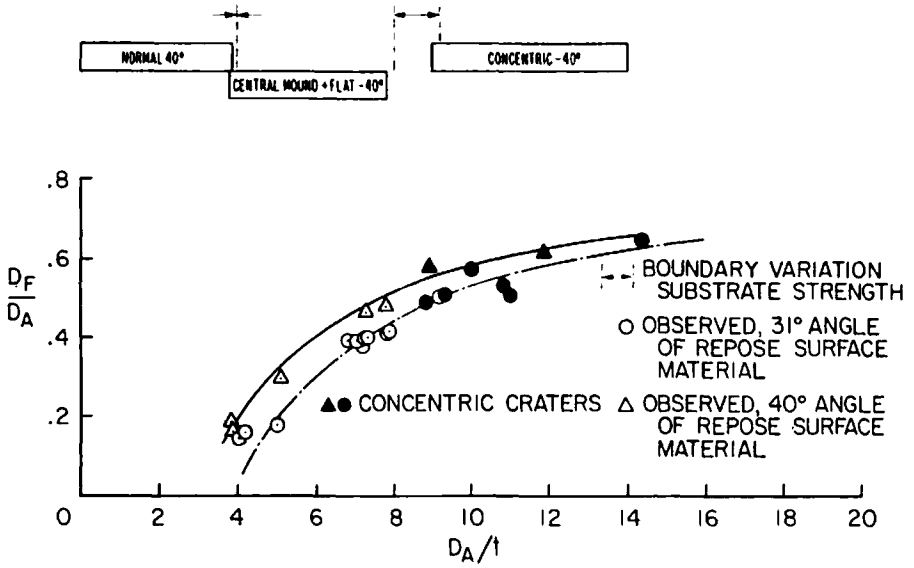

Fig. 6. Comparison of calculated and observed ratios of D_F/D_A plotted as a function of D_A/t. Calculated $D_F/D_A = k - (D_A/t)^{-1}\ 2 \cot \alpha$, where k relates apparent and true diameter and α is the angle of repose of the surficial material. Observed ratios were obtained using surficial materials of 24-mesh quartz sand with a 31° angle of repose and 6- to 8-mesh crushed quartz with a 40° angle of repose.

stant acceleration. Craters of all morphologic es were produced in low gravity fields, approximately $\frac{1}{6}$ g, and stereoscopic pairs of otographs were taken of the craters after the ction process was complete but before the get motion was arrested. Unfortunately, the e available with constant target acceleration s not sufficiently long to permit postejection gravitational adjustment to occur. However, photographs of transient craters forming in a 1-g field could be obtained for craters in the same stage of development as those in the $\frac{1}{6}$-g field, immediately after formation of the crater rim, and D_F/D_A and D_A/t ratios of the transient craters could be compared. The comparisons are shown in Figure 7. The data from transient

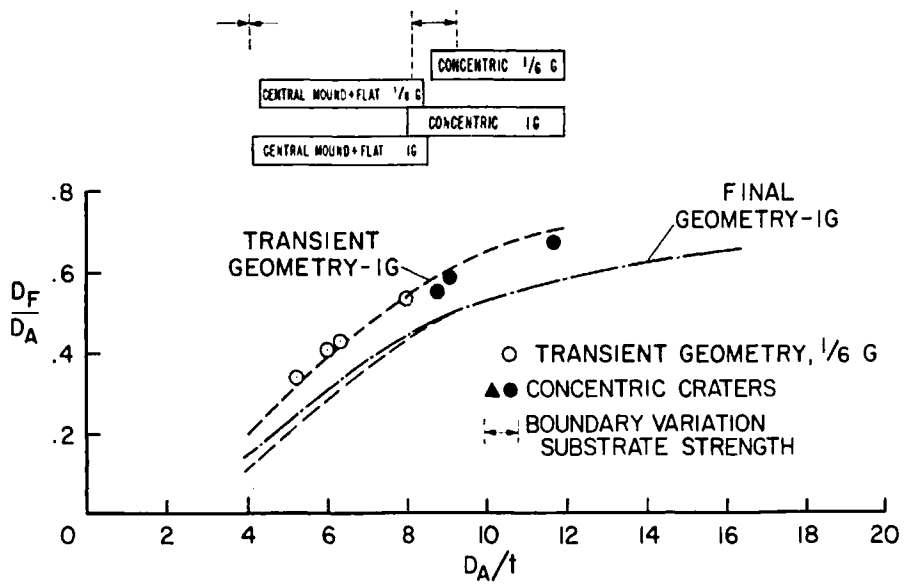

Fig. 7. Relationships between crater geometry and ratios of D_A/t and between ratios of D_F/D_A and D_A/t for 1- and $\frac{1}{6}$-g fields. Dashed curve for craters at postrim development–pregravitational adjustment stage in a 1-g field; points from craters in $\frac{1}{6}$-g field in same stage of development; solid curve for crater geometry after gravitational adjustment in a 1-g field.

craters formed in a ⅙-g field, plotted as points, are compatible with the dashed curve determined from measurements of craters in the same stage of development formed in a 1-g field. The realms of crater morphology for transient craters in the postrim development stage produced in ⅙- and 1-g fields are also shown. The boundary separating normal from central-mound and flat-bottom realms was not examined, but the range of experimental uncertainly of the location of the boundary between the flat-bottomed and concentric realms, $D_A/t = 7.8$ to 8.8, is about the same as the range of variability of that boundary introduced by variations in strength of the substrate. Comparison of final crater geometry was impossible because of the experimental limitations, but, because the angle of repose is not a function of gravity field, it is assumed that the ratios of dimensions of craters produced in ⅙- and 1-g fields would be affected in the same manner by gravitational collapse of the walls to the angle of repose. It is concluded that the magnitude of the gravity field appears to have no effect on boundary values or on the dependence of the ratio D_F/D_A *on* D_A/t for craters in cohesionless sand.

In summary, there appear to be no systematic variations in the dependence of the relationship between D_F/D_A and D_A/t for variations in strength of the substrate, velocity and angle of impact, projectile properties, or gravity field. Variation in velocity and angle of impact, pr jectile type, gravity field, or angle of repose the surfical material does not cause any signi cant variation in positions of boundaries sep rating realms of crater morphology. Strength the substrate is the only variable studied th clearly affects the conditions of formation the various morphologic types of craters, a that effect causes variations only in the positi of the boundary separating flat-bottomed fr concentric geometry.

It is therefore clear that, if laboratory impa data are to be used to determine the thickne of the lunar surface layer, the magnitude of t variations in the position of the bounda values must be determined for realistic ran of possible effective lunar substrate strength. this study, materials with an extremely wi range of strengths were used to obtain t widest possible variation in the boundary co ditions. Most of the laboratory studies we performed using substrate materials with unco fined compressive strengths of 1.4 bars ±30 and 68.5 bars ±5%. To be extremely cautio however, basalt substrates with unconfined co pressive strengths of 2060 bars ±30% we included. Results of these experiments are p sented in Figure 8 for all the substrate ma rials studied under all conditions of angle a velocity of impact and for all projectile ty used. The functional relationship betwe D_F/D_A and D_A/t ratios is clear. The plott

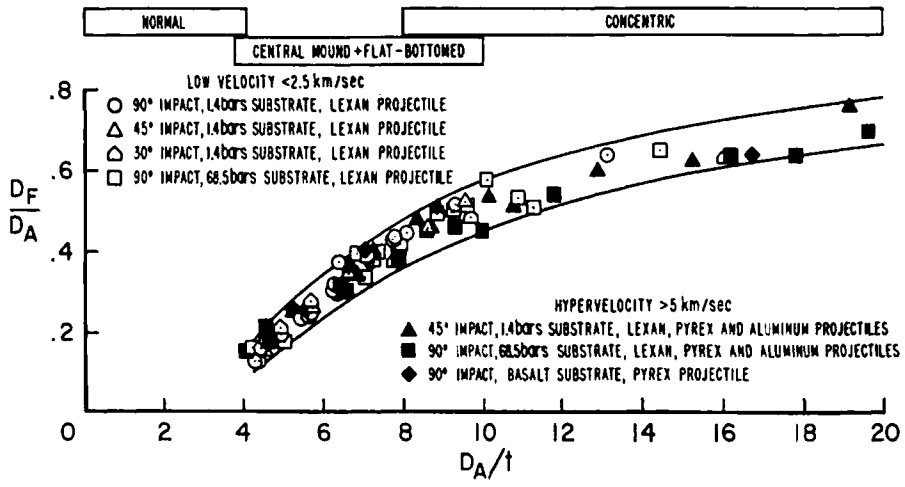

Fig. 8. Summary relationships between crater geometry and ratios of D_A/t and between ratios of D_F/D_A and D_A/t for craters produced by all projectile types impacting at angles between 30° and 90° at velocities from 1 to 7 km/sec against targets with substrates with unconfined compressive strengths ranging from 1.4 to 2060 bars. All craters were formed in a 1-g field in air at pressures of 100 μ and in targets with 24-mesh quartz sand surficial layers.

Fig. 9. F
of known
projectile; i

points scatter
but they are sl
curves. The ma
of the boundary
mound and fla
$D_A/t = 3.8$ to
separating realr
centric geometr
range from D_A/t
in terms of the
variation is grea
of the effects
greater range is
data from expe
substrate materi
tionships betwee
Figure 8 represe
conditions of for
be expected on
offered that the
origin, it will th
gathered in the
Figure 8 to obtai
thickness of the

TEST OF

All the morp
craters discussed
less than a few
cated in the lab
with loose granu
hesive substrates
independent kno
of the lunar surf

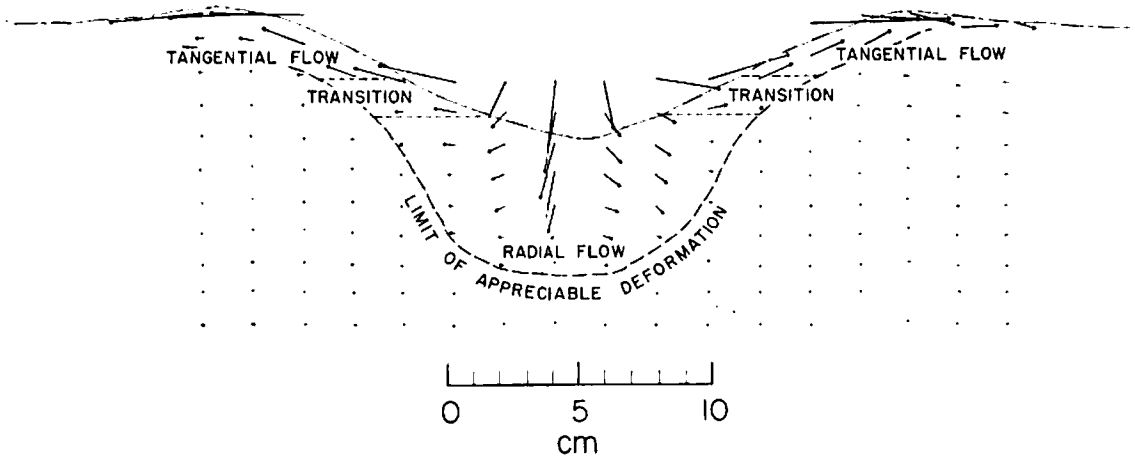

Fig. 9. Flow pattern of granular materials near an impact crater determined from positions of known points within the target materials before and after the crater formed. Pyrex projectile; impact velocity, 0.69 km/sec; angle, 90°.

ints scatter randomly about a single curve, t they are shown here enclosed by limiting rves. The maximum variation in the position the boundary separating normal from central-und and flat-bottomed geometry is from $/t = 3.8$ to $D_A/t = 4.2$. Boundary values arating realms of flat-bottomed from con-tric geometry for all conditions of impact ge from $D_A/t = 8$ to $D_A/t = 10$ or expressed terms of the ratio D_F/D_A 0.48 ± 0.03. This iation is greater than that found in the study the effects of substrate strength, but the ater range is due entirely to the inclusion of a from experiments using extremely strong strate materials. Boundary values and rela-nships between ratios of D_F/D_A and D_A/t of ure 8 represent the widest possible range in ditions of formation of each crater types to expected on the moon. If evidence can be ered that the lunar craters are of impact in, it will then be possible to use the data thered in the laboratory and displayed in ure 8 to obtain documented estimates of the kness of the lunar surface layer.

Test of Impact Hypothesis

All the morphologic types of fresh lunar ters discussed in this paper with diameters than a few hundred meters can be dupli-ed in the laboratory by impacting targets h loose granular layers overlying more co-ive substrates. This evidence coupled with pendent knowledge of the granular nature the lunar surface was so convincing that it was assumed by *Oberbeck and Quaide* [1967] that the lunar craters in question were formed by impact. To test the hypothesis, it is useful to consider the mechanism of formation of the laboratory impact craters having these morphologies.

Gault et al. [1968] have hypothesized that craters produced by the impact of projectiles against homogeneous granular targets are a result of transfer of projectile kinetic energy to the target through shock-wave compression of the target materials followed by the more lengthy process of rarefaction-wave decompression and attendant ejection. They pointed out that particle movement during cratering would always be at an angle to lines perpendicular to the hemispherical shock front expanding through the target. Their evidence offered to confirm this hypothesis is shown in Figure 9, where the flow pattern of granular materials near the crater is depicted as determined from positions of specific points within the target materials before and after the crater formed. It can be seen that below the crater the flow of materials is radial, downward, and nearly perpendicular to the crater surface. The result of this radial flow of material can be seen in Figure 10*A*, where a basin-like depression has been produced in strata beneath the crater. The outward, nearly horizontal grain movements in the zone of transition are responsible for the production of the ring anticline observed at approximately 0.75 of the crater depth. The overturned strata near the rim are the result of material flow in a

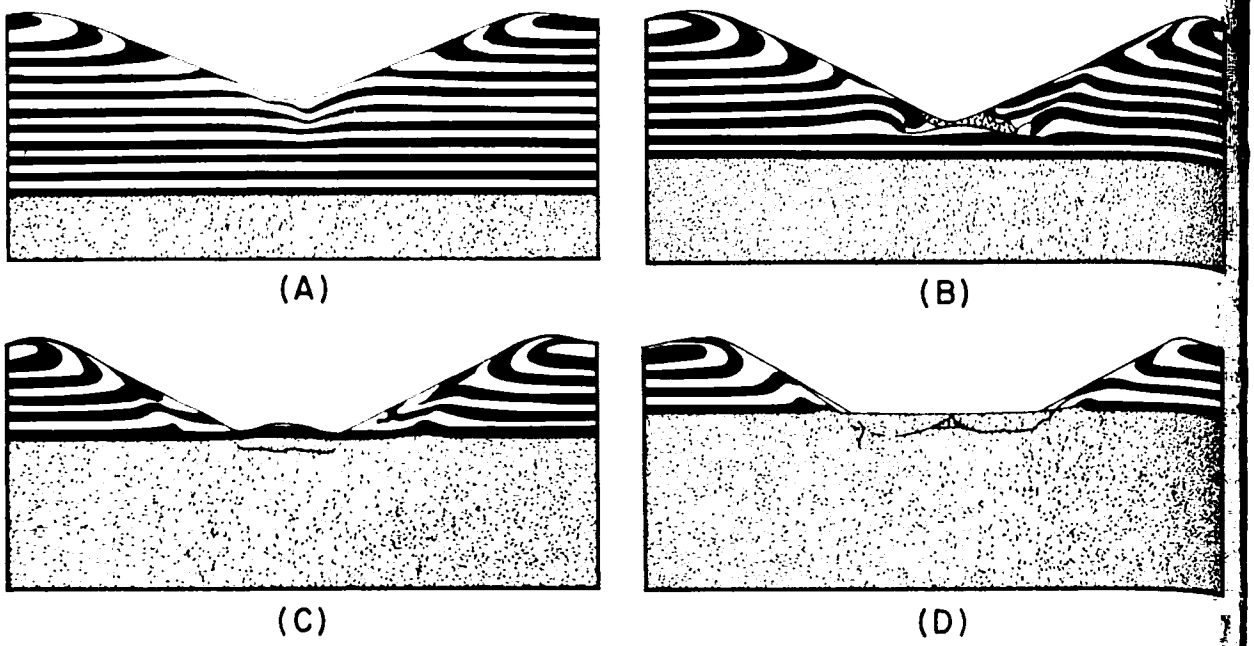

Fig. 10. Near-crater structure of loose, stratiform layers above substrates with unconfined compressive strengths of 1.4 bars ±30%. All craters produced by 1-km/sec normal impacts of 7.65 × 4.00-mm cylindrical Lexan projectiles against surficial materials consisting of loose 24-mesh quartz sand in a 1-g field at air pressures of 100 μ. (A) Normal crater in a thick surficial layer. (B) Normal crater in a thin surficial layer. (C) Central-mound crater. (D) Flat-bottomed crater.

direction tangential to the crater surface, subparallel to the path of ejecta leaving the crater.

When a strong substrate is present at depths less than one crater radius beneath a normal crater, there is less deformation in strata beneath the crater floor but above the substrate. The structure there has been observed to change as the surface layer becomes thinner. The downwarping of the strata continues in regions peripheral to the center of the crater, but in the center the strata are displaced less and less. The end result is the production of a structural dome surrounded by a ring syncline as can be seen in Figure 10B. This structure indicates that the downward component of the radial flow beneath the center of craters in thick granular targets is inhibited when a substrate is present at shallow depths. When the relative thickness of the surficial layer is decreased so that it is slightly less than $D_a/4$, the crater floor becomes flattened.

When the relative thickness of the layer is between $D_a/4$ and $D_a/7.5$, the crater floor is significantly flattened, but a mound is left in the exact center of the crater. Mound height relative to crater depth, a/h, increases with decreasing relative thickness until $t = D_a/6.25$ and then decreases abruptly as shown in Figure 11. A sectional view of a central mound crater is shown in Figure 10C. The mound is similar in structure to the subsurface dome observed beneath normal craters formed in thin surface layers. It appears to have the same origin. The hemispherical shock wave set up in the surficial layer by the impact expands and decays in intensity as it envelops more and more material. When the shock wave reaches the substrate, it can be either partially or totally transmitted. In these studies the bulk density of the substrate is only 5% greater than that of the surficial material. It is assumed, therefore, that the shock wave is in most cases transmitted to the substrate with minimal energy loss because of the approximate density match between the surface layer and substrate. In most central-mound craters the surficial layer is so thick that the shock wave has decayed to such an extent that the pressure of the wave transmitted is less than the dynamic yield strength of the substrate. The substrate remains undamaged and the only observable deformation takes place in the granular surficial layer.

In rare cases in this study the central mound was observed to consist of crushed debris

of the substra
cratered surfic
found only in
having uncon
1.4 bars ±30%
relatively thin,
this kind of
granulated. It
cases the pressu
to the substrate
yield strength
plished by the
sulted in the bu
to produce a
floor.

When the su
$t \leq D_a/7.5$, cer
crater has a fla
present because
at the surficial-
that the pressu
rarefaction wav
granular mater
central region
sufficiently to b
substrates the p
ferred to the su
yield strength:
the surficial lay
large values of
with unconfined
bars ±30% usi
irregular appear
substrates are fr

Fig. 11. R
D_a/t for cent
at velocities
surficial layer
ranging from

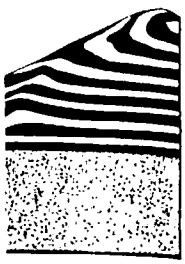

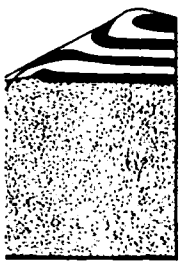

unconfined
impacts of
of loose 21-
ick surficial
) Flat-bot-

Figure 11. A
ound crater is
id is similar in
e observed be-
n thin surface
me origin. The
in the surficial
l decays in in-
more material.
ie substrate, it
transmitted. In
he substrate is
surficial mate-
hat the shock
ed to the sub-
because of the
ween the sur-
central-mound
thick that the
an extent that
mitted is less
n of the sub-
damaged and
takes place in

· the central
crushed debris

the substrate rather than of residual unitered surficial material. These mounds were und only in craters produced over substrates ving unconfined compressive strengths of bars ±30% where the surficial layer was latively thin, $t < D/7$. The substrate beneath is kind of central mound is fractured and anulated. It is hypothesized that in these ses the pressure of the shock wave transmitted the substrates was greater than their dynamic ld strength and that pressure release accomshed by the trailing rarefaction waves reted in the bulking of the granulated material produce a mound of debris on the crater or.

When the surficial layer is sufficiently thin, $\leq D_A/7.5$, central mounds never form and the ater has a flat floor. The mound is no longer esent because the pressure of the shock wave the surficial-substrate boundary is so great at the pressure release accomplished by the refaction waves is sufficient to cause all the anular material above the substrate in the ntral region of the crater to be accelerated fficiently to be ejected. In targets with strong bstrates the pressure of the shock wave transrred to the substrate is less than its dynamic ld strength; hence, cratering is restricted to surficial layer. Flat-bottomed craters with ge values of D_A/t produced over substrates th unconfined compressive strengths of 1.4 rs ±30% usually have cracked or slightly egular appearing floors. In these cases the bstrates are fractured and granulated as illustrated in Figure 10*D*. The pressure of the shock wave transmitted to the substrate in these cases is greater than the dynamic yield strength, but pressures behind the shock front are not sufficiently great to permit acceleration of the granulated materials by the pressure release accomplished by trailing rarefaction waves. Steroscopic pairs of photographs of transient, flat-bottomed craters reveal that the crater walls have a convex shape during early stages of growth, steepening downward, meeting the flat floor along a clearly defined line. The transient crater walls have slope angles greater than the angle of repose. The walls begin to collapse after ejection is complete. This phase of gravitational adjustment takes place over a period of time approximately 10 times that required for crater formation. The final crater walls have slopes equal to the angle of repose of the surficial material.

Concentric craters form when the surficial layer is so thin that the energy transmitted to the substrate is sufficient to produce a crater. Craters in the surficial layer and in the substrate grow almost simultaneously, but the surficial crater grows to a greater size. It is hypothesized that the shock wave generated by the impact of the projectile is transmitted through the surface layer and across the boundary into the substrate, but now the pressure behind the shock front is much greater than the dynamic yield strength of the substrate materials. The materials are consequently granulated. Relaxation from the highly compressed state

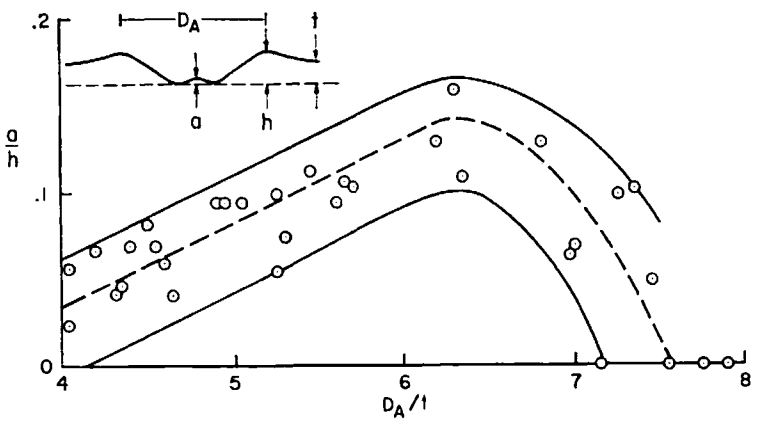

Fig. 11. Relationships between ratios of central-mound height to crater depth (a/h) and D_A/t for central-mound crater formed by projectiles of Pyrex, aluminum, and Lexan impacting at velocities between 1 and 7 km/sec and at angles between 30° and 90° against targets with surficial layers of 24-mesh quartz and lying on substrates with unconfined compressive strengths ranging from 1.4 to 2060 bars. All craters were formed in a 1-g field in air at pressure of 100 μ.

TABLE 2. Energy Balance for the Formation of Concentric Craters

KE_P, $\times 10^9$ ergs	Md at KE_P Sand Target, grams	Md KE_P Surface Crater Layered Target, grams	ΔMd, grams	ΔMd Energy Equivalent from Impact in Loose Sand, $\times 10^9$ ergs	Md 68.5-bar Substrate Predicted from Energy Equivalent and Lab Data, grams	Md 68.5-bar Substrate Observed, grams
8.0	810	104	706	6.1	5.5	5.1
8.5	830	239	591	4.2	3.0	5.2
10.4	920	133	785	7.6	9.5	4.0
7.5	780	103	677	5.5	8.5	7.5
87.0	2600	839	1761	38.0	39.0	29.0
7.5	780	619	161	0.3	0.7	2.6
8.0	810	212	598	4.3	5.9	5.7
9.5	880	150	730	6.5	8.5	3.0
10.6	930	246	684	5.9	8.0	13.0
14.5	1080	142	938	10.8	13.0	8.0

effected by trailing rarefaction waves generated at the free surface of the target results in ejection of the crushed material in a manner similar to that in homogeneous sand targets. There is a difference in size of the inner and outer craters because of differences of the dynamic strengths of the surficial and substrate materials. That is, part of the energy transferred to the substrate is expended in breaking the bonds of the stronger materials. The data of Table 2 support this hypothesis. The difference in mass displaced from a crater produced by impact against a completely homogeneous sand target (column 2) and the mass displaced from that part of a concentric crater above the substrate produced by an impact of the same energy (KE_P in column 3) can be used to determine the estimated energy transferred to the substrate. This estimate is made by equating the difference in mass displaced (column 4) to energy (column 5) through consideration of relationships of mass displaced and energy obtained in studies of impact against homogeneous sand targets. The estimated energy transmitted can then be used with relationships of mass displaced and energy obtained in studies of impact directly against substrate materials to predict the mass displaced from the substrate craters (column 6). The predicted mass displaced compares favorably with the observed mass displaced (column 7). Two conclusions are evident. Although there is not always agreement between the observed and predicted values of mass ejected from the substrate in the formation of a concentric crater, the data clearly suggest that the ma ejected and thus the size of the substrate crat is related to the strengh of the substrate a that transmission of the shock wave to t substrate occurs with minimal energy loss.

The relative sizes of the inner and out crater do not remain constant for different ta get conditions, however. Studies have sho that the ratio of apparent diameters of the in and outer craters, D_I/D_A, increases as the ra D_A/t increases because more and more ener is available for cratering the substrate. Th relationship is shown in Table 3 for concent craters produced in targets with substrates wi unconfined compressive strengths of 1.4 ba ±30% and 68.5 bars ±5%. These data in cate not only that the relative size of the in crater increases with increasing values of t ratio D_A/t but also that the relative size central craters increase with decreasing su strate strength.

Comparison of Laboratory and Lunar Craters

It is now instructive to examine the detail morphology and surface structure of small lu craters and compare them with the same pr erties of laboratory impact craters. Whe possible the observations are from the Lu Orbiter 2 P13 site southwest of Kepler, region chosen for study because of the clar of form of the surface features. Only fr craters were studied, the criteria of fresh

being sharpne
ber of superpo
Craters witl
diameters less
have bowl or
oped rim. Th
depth ratio is
shadows in c
under different
is essentially t
laboratory cra
present at sha
closely to the
depth ratio of
sand targets in
concentration o
than 2 meters
Lunar centr
modal diamete
and a flattene
mound in the
bottomed crate
eters. Their fo
with a slightly
craters slope ev
2°. The flat flo
larger craters it
cracked appear
concentration o
the rims or ejec
and flat-bottom
The concentri
ten of meters to
are characterize
crater. Both out
commonly polyg
ejecta aprons c
diameters signifi

TABLE

D_A/t	Obse
8–10	
10–12	
12–14	
14–16	
16–18	
18–20	

ng sharpness of form and a minimum num- of superposed craters.

Craters with normal geometry usually have meters less than a few tens of meters. They ve bowl or conical shapes with a well-devel- d rim. The average apparent diameter to pth ratio is 5 as determined from studies of adows in craters of many different areas der different angles of illumination. This value essentially the same as the ratio of normal boratory craters formed when substrates are sent at shallow depths, and it corresponds sely to the average apparent diameter to pth ratio of craters produced in homogeneous d targets in the laboratory, 4.4. There is no ncentration of blocks with dimensions greater an 2 meters on the rims of normal craters.

Lunar central-mound craters have larger odal diameters. They have a prominent rim d a flattened floor with the characterizing ound in the center of the crater. The flat- ttomed craters have still larger modal diam- rs. Their form is that of a truncated cone h a slightly raised rim. The walls of fresh ters slope evenly inward at angles of 31° ± The flat floor is often smooth, but in the ger craters it may be hummocky and have a cked appearance. There appears to be no ncentration of blocks 2 meters or larger on rims or ejecta aprons of the central-mound flat-bottom craters.

The concentric craters range in diameter from of meters to several hundred meters. They characterized by low rims and a central ter. Both outer an dinner craters are most mmonly polygonal in plan. Their rims and cta aprons contain abundant blocks with meters significantly greater than the diam- eters of blocks seen elsewhere on the adjacent surface. The blocks in the debris aprons are sometimes displayed in fan-like arrays. The fans become narrower toward the crater and can be traced to the rim of the inner crater, suggesting that the inner crater is the source of the blocks. Thus, as is the case with all the other morphologic types of craters, the morphology and surface structure of the concentric craters is identical to that of their laboratory counterparts. These observations strengthen the validity of the hypothesis that the lunar craters in question are of impact origin.

It is possible to test further the hypothesis by comparing relationships of ratios of measurements made on both lunar and laboratory craters. A large number of lunar concentric craters were studied. Ratios of apparent inner to outer crater diameter, D_I/D_A, and diameter of the surficial crater floor to apparent diameter, D_F/D_A, were determined. These data have been grouped into classes of D_F/D_A values, and the mean and standard deviation of the corresponding D_I/D_A ratios were determined. The relationship between these ratios is shown in Figure 12. The size of the inner crater relative to that of the outer crater increases as D_F/D_A increases. Laboratory data are also shown for comparison. For any given values of D_F/D_A, the D_I/D_A ratio for a lunar concentric crater is higher than the ratio for a laboratory crater in the 68.5-bar substrate and equal to or lower than the ratio for a laboratory crater in the 1.4-bar substrate. The fact that the material strengths used in the laboratory give D_I/D_A ratios that bracket the values observed on the moon indicates that the laboratory strength range of 1.4 to 68.5 bars is adequate for inter-

TABLE 3. Relationship between D_I/D_A and D_A/t for Concentric Craters Formed in Targets with 1.4- and 68.5-bar Substrates

D_A/t	1.4-bar ± 30% Substrate			68.5-bar ± 5% Substrate		
	Observations	Mean D_I/D_A	Standard Deviations	Observations	Mean D_I/D_A	Standard Deviations
-10	7	0.303	0.087	3	0.142	0.087
-12	0			3	0.215	0.040
-14	2	0.503	0.141	1	0.250	
-16	2	0.385	0.095	1	0.266	
-18	0			4	0.324	0.037
-20	0			2	0.358	0.096

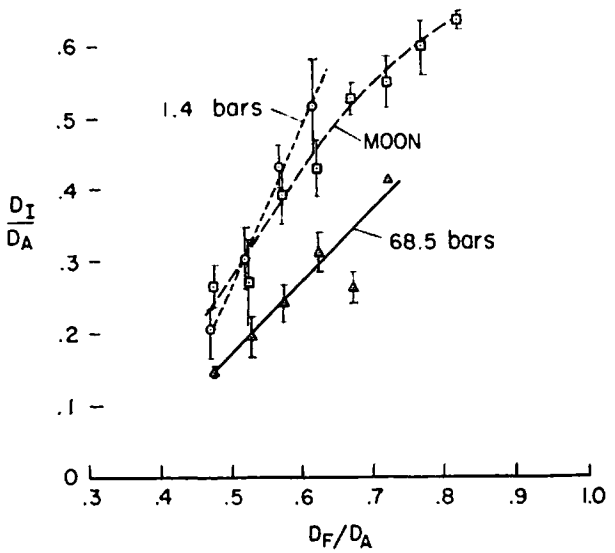

Fig. 12. Relationships between ratios of apparent inner to outer crater diameters, D_I/D_A, and ratios of D_F/D_A for lunar concentric craters in the Lunar Orbiter 2 P13 site and for laboratory concentric craters. Bar lengths represent one standard deviation of the D_I/D_A ratios in each class of D_I/D_A ratios.

pretive purposes to characterize the conditions of formation of the small lunar craters considered in this study. This does not mean that the lunar substrate has an unconfined crushing strength in this range. It indicates only that lunar craters with diameters from 20 to 100 meters could be modeled in this laboratory study using substrate materials with strengths within this range. The similarity of the functional dependence of the relative size of the inner and outer craters on the values of the ratio D_F/D_A for both lunar and laboratory impact craters is strongly suggestive of an impact origin for the lunar concentric craters.

The identity of relationships between D_F/D_A ratios and geometry of lunar and laboratory craters further supports the hypothesis that the lunar craters considered were formed by impact. Measurements of D_F/D_A ratios of more than 100 well-defined flat-bottomed and concentric lunar craters indicate that the value of D_F/D_A representing the boundary between flat-bottomed and concentric craters is 0.5 ± 0.05. The value for the same boundary obtained in the laboratory for all conditions of impact is 0.48 ± 0.03. The fact that the lunar and laboratory craters have this boundary in the same range of D_F/D_A values is convincing evidence that the lunar craters were formed by impact. The authors know of no other natural proce that would account for this agreement. Fo example, there is no reason why the onset central crater formation in any volcanic proc ess should be related to the same ratio of D_F/D The excellent agreement between the lunar an laboratory data indicates that the substrate chosen for this study are in the proper effec tive strength range.

The final and most conclusive supportin evidence of an impact origin of this group c craters is that the distribution of lunar con centric craters can be predicted from the ob served distribution of lunar normal craters an conditions of formation of normal craters de termined in the laboratory. Boundary ratio separating normal from flat-bottomed crate regimes determined in the laboratory were use to estimate the thickness distribution in th Lunar Orbiter 2 P13 site from the observed di tribution of normal craters. The predicted per centages of concentric craters as a function diameter were then calculated using the est mated statistical thickness distribution an experimental boundary values of D_A/t separ ing realms of flat-bottomed from concentri crater morphology. The predicted and observe concentric crater distributions for this area shown in Figure 13. Agreement between t predicted and observed distributions could obtained only if most of the lunar craters co sidered are of impact origin.

Evidence offered in support of the impa hypothesis is summarized below.

1. The form and surface structure of nor mal, central-mound, flat-bottomed and con centric craters on the moon are identical to form and surface structure of normal, centra mound, flat-bottomed, and concentric crate produced in the laboratory by impact again targets consistent with present day knowled of the lunar surface.

2. The dependence of D_I/D_A ratios on va ues of D_F/D_A ratios is similar for concentr craters formed on the moon and for concentr craters produced by impact in the laborator

3. The boundary values of D_F/D_A separat flat-bottomed from concentric craters is simi for lunar and laboratory impact craters.

4. The per cent to size relationship of type of lunar crater can be predicted from

per cent to si
of lunar crate
from laborator

The weight is concluded t craters is of imp

DETERMI

Evidence has craters consider origin. It has be variable studied on the condition logic types of cr of the substrate, enough to introd surface thickness tory impact data used to interpre of the lunar su tribution of the lunar craters in *beck and Quaid* determined boun realms of differe be used, however effect of angle Lunar Orbiter p angles of illumin repose of the lur the walls of flat- equal to the ang

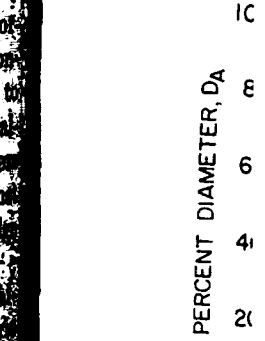

Fig. 13. Obs P13 site and a predicted from in the laborato

per cent to size relationship of another type of lunar crater using parameters determined from laboratory impact experiments.

The weight of evidence is overwhelming. It is concluded that this group of small lunar craters is of impact origin.

Determination of Thickness of Surface Layer

Evidence has been offered that the lunar craters considered in this study are of impact origin. It has been shown further that the only variable studied that has any significant effect on the conditions of formation of the morphologic types of craters in question is the strength of the substrate, but this effect is not extensive enough to introduce large uncertainty in lunar surface thickness determinations. The laboratory impact data of Figure 8 can therefore be used to interpret the distribution of thickness of the lunar surface layer from the size distribution of the various morphologic types of lunar craters in the manner described by *Oberbeck and Quaide* [1967]. The experimentally determined boundary values of D_A/t separating realms of different crater morphology cannot be used, however, without consideration of the effect of angle of illumination. Most of the lunar Orbiter photographs were taken with angles of illumination less than the angle of repose of the lunar surface materials. Because the walls of flat-bottomed craters have slopes equal to the angle of repose of the surficial materials, the flat-bottomed craters with the smallest floor diameters will not be recognized as such when the angle of illumination is less than the angle of repose. Their shadow patterns will be similar to the shadow patterns of normal craters. It is possible to calculate the minimum value of D_F/D_A for recognition of flat-bottomed geometry from the shadow pattern for any angle of repose and angle of illumination. The D_F/D_A value so calculated represents the recognition boundary separating normal from flat-bottomed geometry. If it is assumed that the limit of recognition is the condition for which the shadow cast by the sunward crater rim completely fills the flat floor, as illustrated in Figure 14.1,

$$\tan \gamma = h/(h \cot \alpha + D_F) \qquad (1)$$

where h is apparent crater depth, γ is angle of illumination, and α is angle of repose.

Solving for D_F, we find

$$D_F = (h - h \cot \alpha \tan \gamma)/\tan \gamma \qquad (2)$$

Since $D_A = 2h \cot \alpha + D_F$,

$$\frac{D_F}{D_A} = \frac{1 - \cot \alpha \tan \gamma}{1 + \cot \alpha \tan \gamma} \qquad (3)$$

The recognition boundary in terms of D_F/D_A can be calculated from expression 3 and expressed in terms of the ratio D_A/t by reference to Figure 8. For example, with an angle of illumination of 20.5° and an angle of repose of 31°, the lower limit of recognition of flat-

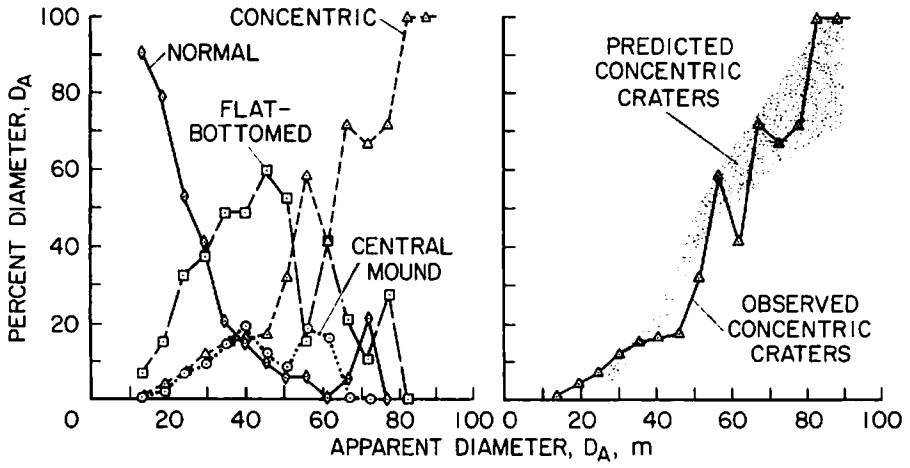

Fig. 13. Observed relationships between size and morphology of craters in Lunar Orbiter 2 P13 site and a comparison of the observed distribution of concentric craters with a distribution predicted from the distribution of normal craters and boundary values of D_A/t determined in the laboratory.

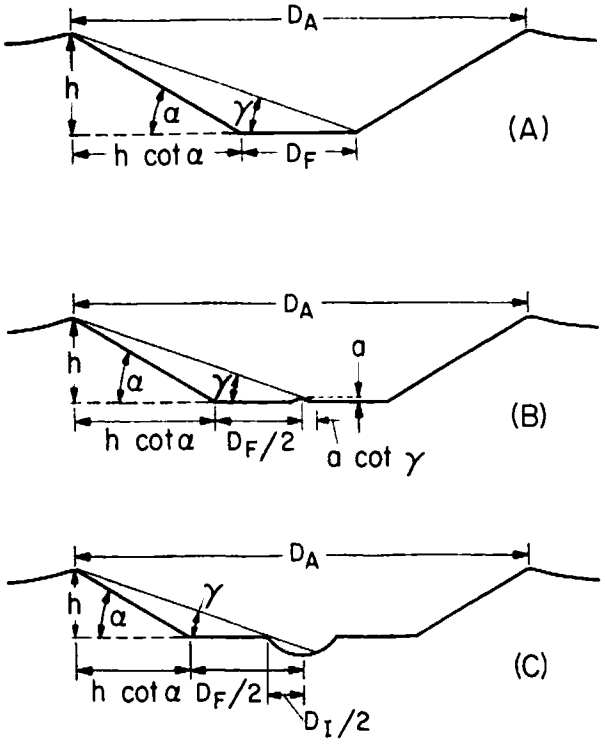

Fig. 14. Crater geometry defining the lower limit of recognition from cast shadows for (*A*) flat-bottomed craters, (*B*) central-mound craters, and (*C*) concentric craters.

bottomed geometry is, in terms of the ratio D_F/D_A, 0.23. From the curve in Figure 8, a value of D_F/D_A of 0.23 corresponds to values of D_A/t ranging from 4.8 to 5.7, the lower range of recognition of flat-bottomed geometry at this illumination angle.

From laboratory experiments it was demonstrated that central-mound craters form at values of D_A/t ranging from 4.0 to 7.5 for all conditions of impact. Recognition of a central mound in a flat-bottomed lunar crater depends, however, on the angle of illumination and height of the mound relative to the crater walls. For a mound to be seen, it must be free of or extend through the shadow cast by the sunward rim of the crater. The lower limit of recognition is defined as the geometry for which the cast shadow just covers the central mound, as illustrated in Figure 14*B*. From Figure 14*B*

$$\tan \gamma = \frac{h}{h \cot \alpha + D_F/2 + a \cot \gamma} \tag{4}$$

Solving for D_F, we have

$$D_F = \frac{2(h - h \cot \alpha \tan \gamma - a)}{\tan \gamma} \tag{5}$$

Since $D_A = 2h \cot \alpha + D_F$,

$$\frac{D_F}{D_A} = \frac{h - (h \cot \alpha \tan \gamma + a)}{h - a} \tag{6}$$

Laboratory studies summarized in Figure 1[illegible] indicate that the smallest central mound tha[illegible] was detected had a height a equal to 0.05 [illegible]

For the limiting case, a approaches 0

$$\lim_{a \to 0} D_F/D_A = 1 - (\cot \alpha \tan \gamma) \tag{7}$$

Therefore,

$$D_F/D_A = 1 - \cot \alpha \tan \gamma \tag{8}$$

The limiting condition of recognition of a cen[illegible] tral-mound crater can be calculated for an[illegible] illumination angle from expression 8. For e[illegible] ample, the Lunar Orbiter 2 P13 site has [illegible] average illumination angle of 20.5° and a mea[illegible] ured angle of repose of 31°. The calculat[illegible] lower limit of recognition occurs when the ra[illegible] $D_F/D_A = 0.37$. From Figure 8 this ratio co[illegible] responds to a minimum ratio of D_A/t of 6[illegible] The upper limit of recognition is the expe[illegible] mental upper limit of formation, $D_A/t = 7$[illegible]

Laboratory experiments indicate that wi[illegible] varied experimental conditions the bounda[illegible] between the flat-bottomed and concentric cra[illegible] regimes ranges between $D_A/t = 8$ and D_A/t [illegible] 10. The recognition boundary between flat-b[illegible] tomed and concentric craters is the experimen[illegible] boundary for illumination angles greater th[illegible] 20°. In a derivation similar to that for centr[illegible] mound craters, the minimum value of $D_F/$[illegible] can be calculated, which represents the con[illegible] tion at which the shadow cast by the ou[illegible] crater rim just touches the rim of the in[illegible] crater, as illustrated in Fig. 14*C*. This rep[illegible] sents the limiting condition of recognition [illegible] cause the most characteristic and often the o[illegible] criterion for recognition of a small cen[illegible] crater is the shadow pattern or albedo dif[illegible] ence on the sunward side of the inner cra[illegible] It can be seen from Figure 14*C* that

$$\tan \gamma = \frac{h}{h \cot \alpha + D_F/2 - D_I/2}$$

Since the smallest central crater prod[illegible] under all conditions of impact in the labora[illegible] has an apparent diameter, D_I of $0.33D_F$[illegible] can be written in terms of D_F and expre[illegible] 9 can be solved for D_F:

D_F

Since $D_A =$

$\frac{D_F}{D_A} =$

From this e
for the recogn
bottomed fron
for any illumin
For example, i
with an averag
a measured ang
condition of re
is $D_F, D_A =$ (
ratio of 0.48 c
D_A/t ranging f
mental bounda
than 20.5° give
aries separating
concentric geom
perimentally d
cases when the
is less than th
whatever geom
is the experimer

It is thus po
nition boundari
separating all th
of craters recogn
types can now
the recognition
tribution of thic
Thickness deter
concentric crate
the midpoint di
terval by maxin
the respective b
point diameters
divided by the
indicating that th
craters of this di
some value with
similar manner,
class of concentr
cating that the la
value between t
obtained.

A specific rang
mined theoretical
crater size class

$$D_F = \frac{h(1 - \tan\gamma \cot\alpha)}{0.33 \tan\gamma} \quad (10)$$

Since $D_A = 2h \cot\alpha + D_F$,

$$\frac{D_F}{D_A} = \frac{1 - \tan\gamma \cot\alpha}{1 - 0.33 \tan\gamma \cot\alpha} \quad (11)$$

From this expression it is possible to solve r the recognition boundary separating flat-ttomed from concentric regimes of craters r any illumination angle and angle of repose. or example, in the Lunar Orbiter 2 P13 site, ith an average illumination angle of 20.5° and measured angle of repose of 31°, the limiting ndition of recognition for a concentric crater $D_F/D_A = 0.48$. From Figure 8, a D_F/D_A tio of 0.48 corresponds to possible values of $_A/t$ ranging from 8 to 10, the exact experi-ental boundaries. Illumination angles greater an 20.5° give calculated recognition bound-es separating regimes of flat-bottomed from ncentric geometry that are less than the ex-rimentally determined values. Thus, in all es when the calculated recognition boundary less than the experimental boundary, for atever geometry, the recognition boundary the experimental boundary.

It is thus possible to determine the recog-ion boundaries in terms of the ratio D_A/t parating all the realms of morphologic types craters recognized. The distribution of crater pes can now be interpreted on the basis of e recognition boundaries to obtain the dis-bution of thickness in the area considered. hickness determinations using normal and ncentric craters are obtained by dividing e midpoint diameter of each crater size in-val by maximum and minimum values of e respective boundary ratios. Thus, the mid-int diameters of a size class of normal craters vided by the boundary values gives a result dicating that the layer thickness sampled by aters of this diameter interval is greater than me value within the range obtained. In a nilar manner, the calculation using a size ss of concentric craters gives a result indi-ting that the layer thickness is less than some lue between the maximum and minimum tained.

A specific range of thickness can be deter-ned theoretically in the same way for each ter size class of central-mound craters and for each size class of flat-bottomed craters. In practice, however, these two groups of craters must be considered together because central-mound craters in each size class with small D_A/t ratios are not recognized as such and are, instead, recognized at flat-bottomed craters. Thus, the flat-bottomed craters in every size class have two possible ranges of limiting D_A/t ratios. This situation is avoided by combining the two groups. A specific range of thickness sampled by each size class of this combined group can be determined by dividing the mid-point diameter of each size class by the upper and lower boundary values.

To determine the statistical distribution of thickness in an area, the proportion of one or more crater types to all other crater types in each size interval must be considered. If the craters are assumed to be randomly distributed, the proportion of normal craters in a given size class indicates the proportion of area sampled by that size class interval with a thickness greater than the values obtained by dividing the class midpoint diameter by the boundary values of the ratio D_A/t. The proportion of concentric craters in the size class interval indicates the proportion of area samples by craters in that interval with a thickness less than the values obtained by dividing the size class mid-point diameter by the boundary values of the ratio D_A/t. The proportion of central-mound plus flat-bottomed craters in the interval gives the proportion of area with a thickness between the limits obtained by dividing the size class midpoint by the upper and lower boundary values of the ratio D_A/t. The proportion of the area with thickness greater than t determined from the proportion of normal craters in any one size class interval is equal to the complement of the proportion of the area with thickness less than t determined from the proportion of all other crater types in the same size class. Conversely, the proportion of area with thickness less than t determined from the proportion of concentric craters in any one size class interval is equal to the complement of the proportion of area with thickness greater than t determined from the proportions of all all other types of craters in that size class. The results of the calculations can therefore be presented simply in terms of proportions of normal and concentric craters together with the

TABLE 4. Calculated Per Cent Area Thickness Distribution of Fragmental Surface Layer in Lunar Orbiter 2 P13 Si

D_{MP} Midpoint, Diameter Interval Meters	N All Craters	Normal Craters: n Normal Craters	Normal Craters: n/N % Normal Equals % Area	Normal Craters: 90% Conf. Interval % Area	Normal Craters: t, meters, > range $D_{MP}/5.7$	Normal Craters: t, meters, > range $D_{MP}/4.8$	Concentric Craters: n Conc. Craters	Concentric Craters: n/N % Conc. Equals % Area	Concentric Craters: 90% Conf. Interval % Area	Concentric Craters: t, meter < rang $D_{MP}/10$	D
13.4	3264	2976	91.7	90.8–92.5	2.35	2.8	28	0.9	0.1–13.1	1.3	
18.7	1509	1193	79.0	77.0–81.0	3.3	3.9	51	3.4	0.6–11.8	1.9	
24.1	743	393	52.9	48.6–57.1	4.2	5.0	52	7.0	2.5–16.4	2.4	
29.4	257	110	41.2	33.3–49.5	5.15	6.1	32	12.0	4.4–26.3	2.9	
34.8	180	38	21.1	11.3–35.2	6.1	7.2	27	15.0	5.8–31.6	3.5	
40.1	128	18	15.2	4.5–36.7	7.0	8.3	19	16.1	5.1–36.9	4.1	
45.5	81	8	9.9	0.3–45.0	8.0	9.45	14	17.3	4.5–42.6	4.55	
50.8	34	2	5.9	4.2–78.6	8.9	10.6	11	32.3	11.8–61.1	5.1	
56.2	32	2	6.2	4.0–78.8	9.85	11.7	19	59.4	38.4–77.7	5.6	
61.5	12	0	0.0		10.8	12.8	5	41.7	9.8–80.7	6.15	
66.9	18	1	5.5	16.3–94.1	11.7	13.9	13	72.2	45.6–89.8	6.7	
72.2	9	2	22.2	0.1–86.7	12.65	15	6	66.7	28.1–92.6	7.2	
77.6	7	0	0.0		13.6	16.1	5	71.4	28.3–95.9	7.8	
82.9	5	0	0.0		14.5	17.2	5	100	53.3–96.5	8.3	10
88.3	4	0	0.0		15.5	18.3	4	100	46.5–95.6	8.8	11
93.8	4	1	25.0	3.0–98.0	16.4	19.5	3	75.0	20.2–99.3	9.4	12
99.0	2	0	0.0		17.4	20.6	2	100	24.8–89.8	9.9	12

indicated thickness limits. Because normal craters of each size class sample the proportion of area with thickness greater than t and the concentric craters in each size class sample the proportion of area with thickness less than t and because the limiting thickness sampled by each type of crater varies directly with the diameter, the consideration of all size class intervals over a sufficiently large range of crater diameters gives the cumulative percentage of area with thickness greater or less than the limiting values.

The proportion of central-mound and flat-bottomed craters in each class cannot be used to determine a unique thickness distribution because the range of thickness determined from adjacent size class intervals overlaps and cannot be cumulated. Results on an analysis of the distribution of thickness of the surface layer using normal and concentric craters in the Lunar Orbiter 2 P13 site are presented in Table 4. The data of Table 4 are presented in cumulative curve form in Figure 15. The plotted information includes the possible ranges of thickness indicated for each determination and 90% confidence limits for the per cent area. The shaded area bounded by curves represents the area within which both groups of data are concordant. The median thickness is in the 5- to 5.5-meter range with 50% of the area havi thickness between 4 and 7 meters. Surface crop appears to be minimal.

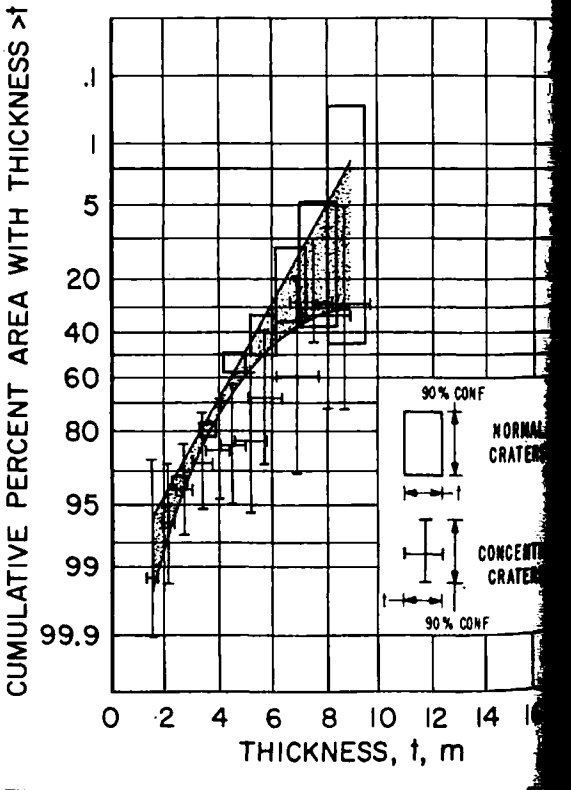

Fig. 15. Cumulative per cent area of the Orbiter 2 P13 site with thickness greater th

The layer thic
cific locations.
making such me
use of the centr
cussed. It has
each central-mo
that the thickne
site of the crate
of values determ
diameter of the
and lower limitin
The other t
D_F/D_A ratios of
vious from the c
ratio of any crate
be fixed within
determine a max
the layer thickn
iently defined t
and D_F. This m
angle of illuminat
of that fact. It
ment of D_F must
pendicular to the
the limiting condi
by the illuminatio
D_F/D_A for which
the flat floor. Th
calculated for ar
Figure 14.1, of wh

$$\tan \gamma =$$

Solving for D_F, v

$$D_F = \frac{2(}{}$$

Since $D_A = 2h$ c

$$D_F/D_A =$$

For example, the
n illumination an
pose of 31°. The
recognition is L
hat, of 104 measu
e P13 site, the
375. From the c
tio of 0.375 corre
D_A/t of 6.5. Th
ement of a $D_F/$
oretically, but it

ıar Orbiter 2 P13 Site

ric Craters

0% onf. erval Area	$D_{MP}/10$	t, meters, < range D_M
-13.1	1.3	1
-11.8	1.9	2
-16.4	2.4	3
-26.3	2.9	3
-31.6	3.5	4.3
-36.9	4.1	5.0
-42.6	4.55	5.7
-61.1	5.1	6.3
-77.7	5.6	7 0
-80.7	6.15	7.7
89.8	6.7	8.4
92.6	7.2	9.0
95.9	7.8	9 7
96.5	8.3	10.4
95.6	8.8	11.0
99.3	9.4	11.7
99.8	9 9	12.4

the area having s
ters. Surface out-

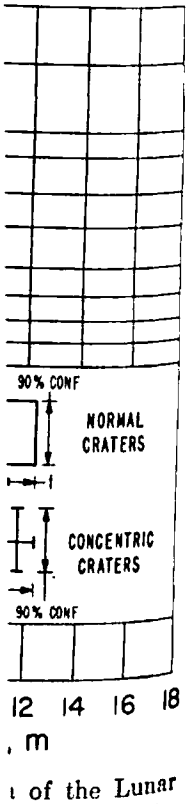

ı of the Lunar
greater than t.

The layer thickness can be measured at specific locations. There are two techniques for making such measurements. One method makes use of the central-mound craters already discussed. It has been demonstrated above that each central-mound crater observed indicates that the thickness of the surface layer at the site of the crater lies within a restricted range of values determined by dividing the apparent diameter of the observed crater by the upper and lower limiting ratios of D_A/t.

The other technique involves measuring D_F/D_A ratios of well-defined craters. It is obvious from the curve of Figure 8 that a D_F/D_A ratio of any crater demands that the D_A/t ratio be fixed within limits. It is thus possible to determine a maximum and minimum value of the layer thickness around any crater sufficiently defined to permit measurement of D_A and D_F. This measurement is affected by the angle of illumination and account must be taken of that fact. It is obvious that the measurement of D_F must be made in a direction perpendicular to the crater-sun line. Furthermore, the limiting condition of measurement imposed by the illumination angle occurs at a value of D_F/D_A for which the shadow covers one-half the flat floor. This limiting condition can be calculated for any illumination angle. From Figure 14.1, of which this is a special case,

$$\tan \gamma = \frac{h}{h \cot \alpha + D_F/2} \tag{12}$$

Solving for D_F, we have

$$D_F = \frac{2(h - h \cot \alpha \tan \gamma)}{\tan \gamma} \tag{13}$$

Since $D_A = 2h \cot \alpha + D_F$,

$$D_F/D_A = 1 - \cot \alpha \tan \gamma \tag{14}$$

r example, the Lunar Orbiter 2 P13 site has illumination angle of 20.5° and an angle of ose of 31°. The calculated limiting condition recognition is $D_F/D_A = 0.375$. It is of note t, of 104 measurements of D_F/D_A ratios in P13 site, the lowest value obtained was 75. From the curve of Figure 8, a D_F/D_A io of 0.375 corresponds to a minimum value D_A/t of 6.5. The maximum limit of measment of a D_F/D_A ratio cannot be defined oretically, but it was found that only rarely was a crater observed that had a D_F/D_A ratio greater than 0.7. Thus, for the measurements made in the Lunar Orbiter 2 P13 site, a practical upper limit of recognition can be defined as $D_F/D_A \approx 0.7$ or $D_A/t \approx 16.0$. Therefore, the craters in this site of which the ratio D_F/D_A was measured were in regions where the surface layer thickness lay within the range $D_A/16$ to $D_A/6.5$.

More than 150 values of thickness were determined for specific locations in the Lunar Orbiter 2 P13 site using the two techniques. The thickness values were plotted on medium-resolution photographs covering an area of 650 km². Each plotted thickness determination is a valid measurement, but a statistical thickness distribution cannot be obtained from this sample by determining the percentage of occurrence of measured thickness intervals because the sample is biased. The range of thickness that can be determined from any central-mound crater or from any D_F/D_A ratio of a crater is a function of the crater diameter. Large craters can measure greater values of thickness than small ones. Because there are many more small craters produced per unit time than large ones, a thickness distribution determined from the percentage of occurrence of thicknesses using craters of all sizes of the same apparent age is biased in terms of smaller values of thickness. This bias is modified by the erosional history of the craters counted. The lifetime of a small crater on the moon is shorter than that of a large one. A large crater will have a fresh aspect far longer than a small one, producing a bias toward greater values of thickness. The two biasing agents operate in an opposite sense but do not necessarily nullify one another. The total effect is that the sample has an unknown bias that would be extremely difficult to remove. The plotted thickness values can be examined for trends in thickness variations or for variations as a function of area sampled, however, if the bias is assumed to be the same everywhere. For example, means and standard derivations of the plotted thickness values were computed for randomly selected 10- and 100-km² areas in the P13 site. The means of the samples are not significantly different whether from 10, 100, or the whole 650 km². Nor does the mean value of thickness of any one 10-km² area differ significantly from that of any other

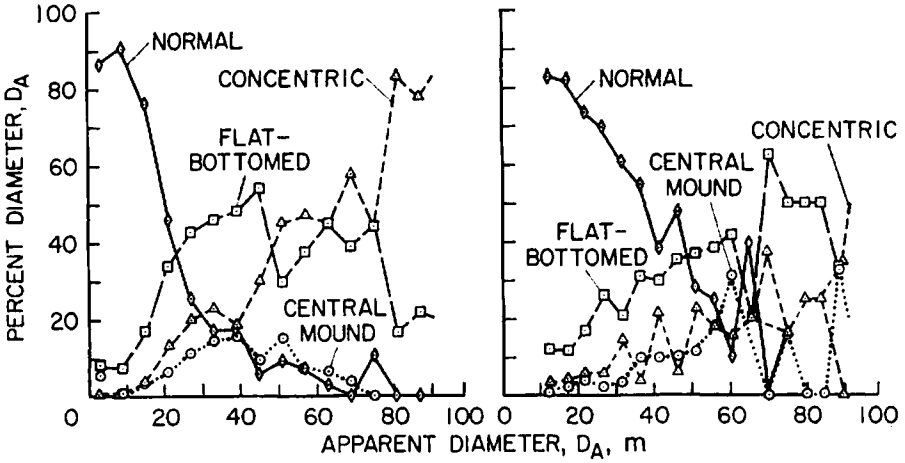

Fig. 16. Relationships between size and morphology of craters in the Lunar Orbiter 3 P12 (*left*) and Lunar Orbiter 2 P7 (*right*) sites.

10-km² area. There are no trends in thickness in the area considered, and the scale of variation of thickness in a 10-km² area is not significantly different from that in the area as a whole.

Statistical thickness determinations using the distributions of normal and concentric craters have also been obtained for the Lunar Orbiter 2 P7 and Lunar Orbiter 3 P12 sites. The crater distributions are shown in Figure 16, and cumulative curves of the thickness are presented in Figure 17. Note again the concordance of the variously determined distributions and the apparent lack of surface outcrop. The surf layer in the Lunar Orbiter 3 P12 site wit the Flamsteed Ring in Oceanus Procellarum slightly thinner than that in the Lunar Orbi 2 P13 site. The median depth is in the 3- 4-meter range with 50% of the area havin thickness between 2.5 and 5.5 meters. This termination is in fair agreement with that ported by *Oberbeck and Quaide* [1967] for same area as determined from medium-res tion Lunar Orbiter 1 photographs (5–6 mete The Lunar Orbiter 2 P7 site in Sinus M on the other hand, has a much thicker sur

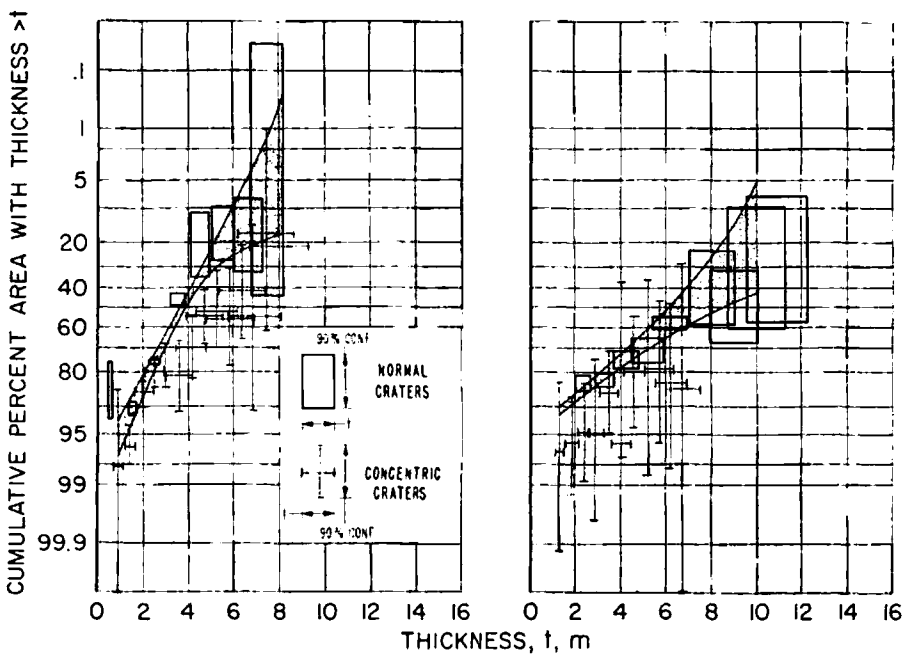

Fig. 17. Cumulative per cent area of the Lunar Orbiter 3 P12 (*left*) and Lunar Orbiter 2 P (*right*) sites with thickness greater than *t*.

layer. The med to 9-meter rang

Only the cra few hundred m this study. Evi is extensive. Th bution of laye niques are so c tain that only been measured. may be delineat to be examined. ured in kilometer and others have without central phology of thes many respects

Fig. 18. Relat 70 and 40

r. The median thickness there is in the 6-
-meter range.

Only the craters with diameters less than a hundred meters have been considered in study. Evidence for an origin by impact extensive. The interpretations of the distribion of layer thickness by different techues are so consistent that it is rather cern that only the surface layer thickness has n measured. Whether or not deeper layers y be delineated by similar methods remains be examined. Craters with diameters measd in kilometers are sometimes flat-bottomed, others have terraced inner walls with or hout central peaks. Admittedly, the morlogy of these craters is grossly similar in y respects to the morphology of craters considered in this study, but there is no indication that the morphology of these craters is due to the same mechanism. On the other hand, there is evidence that the morphology is not due to the same mechanism, even if the large craters were produced by impact. The gross morphology of fresh impact craters with diameters in excess of a few hundred meters no longer reflects differences in the strengths of near-surface rocks. Observations illustrated in Figure 18 suggest that the internal morphology of fresh concentric craters becomes less regular and then less distinct as the diameter increases, until finally the craters have no trace of internal terracing and appear again to have normal morphology. If this sequence is real, it may indicate that, as impact craters become larger,

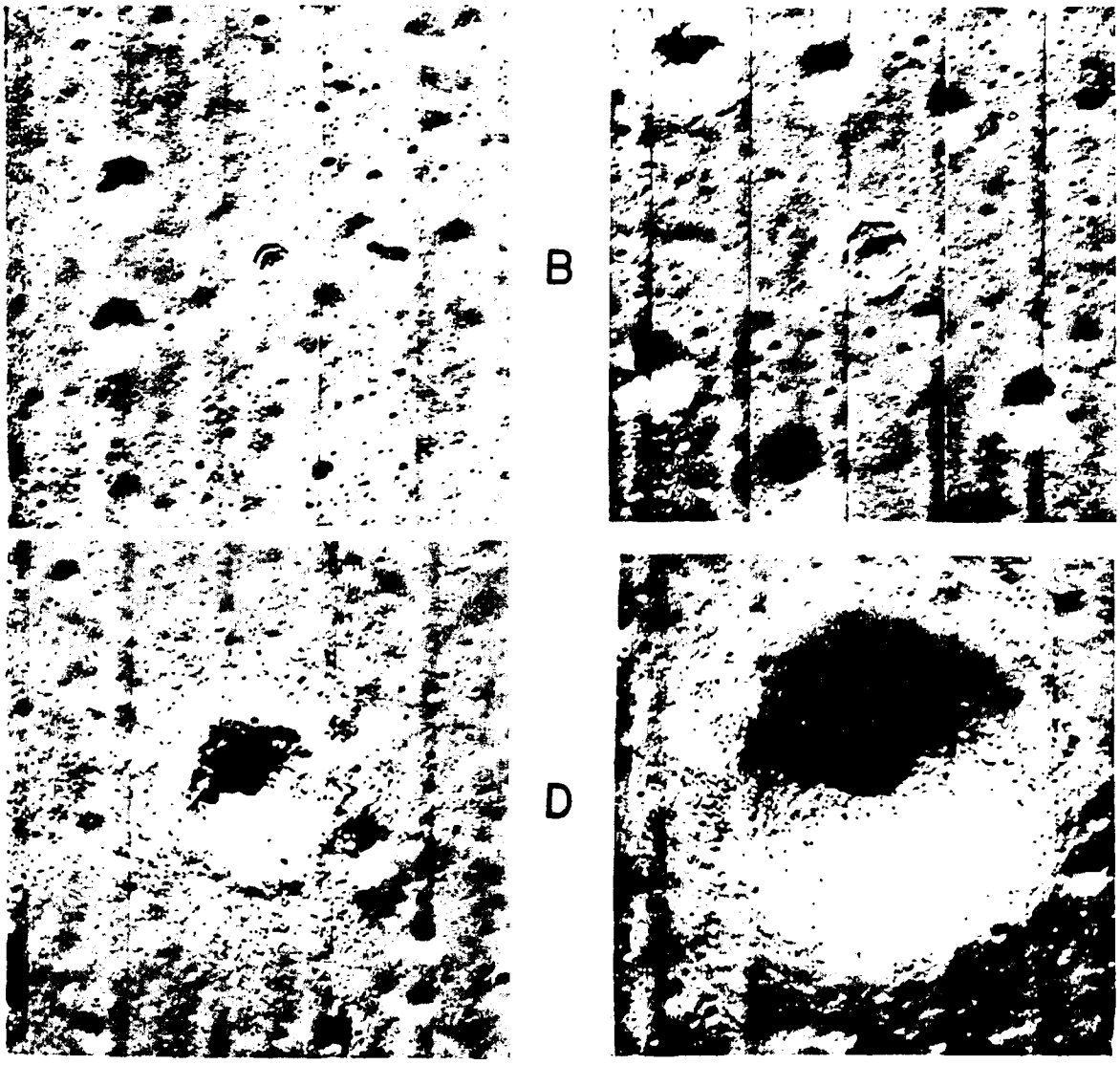

Fig. 18. Relationships between size and morphology of fresh craters with diameters between 70 and 400 meters in an area where the median thickness is of the order of 5 meters.

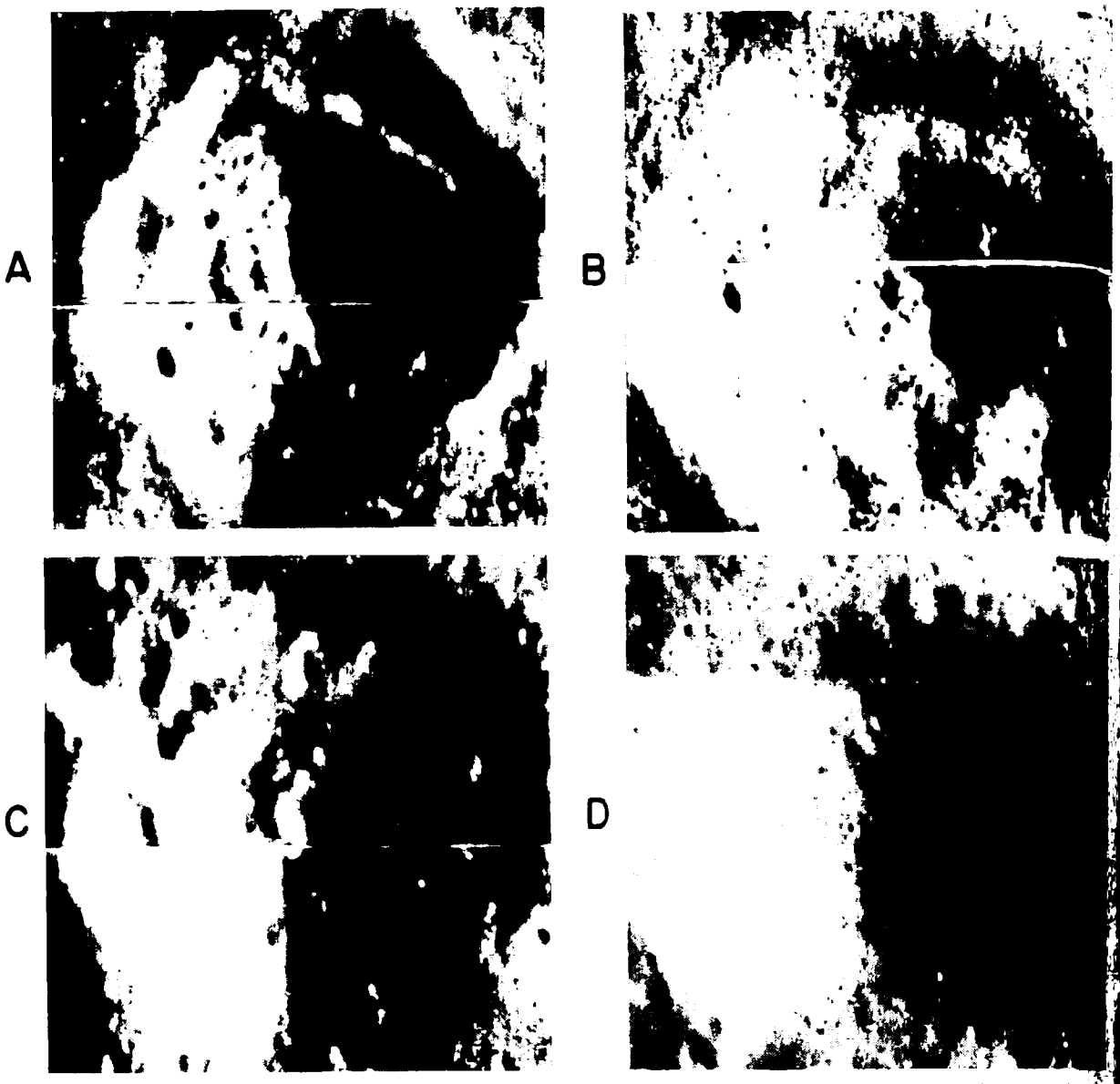

Fig. 19. Interpreted stages of modification of a concentric crater. The craters shown are of the same size (~190 meters) and occur close to one another in a region where the median thickness of the surface layer is of the order of 5 meters. (*A*) Sharply defined concentric crater, square in plan with fans of ejecta blocks originating from the inner crater. Few small craters are superposed on the crater and ejecta. (*B*) Slightly modified concentric crater with square plan shape, inner crater and blocky ejecta still evident. Greater numbers of small superposed craters are present. (*C*) Substantially modified concentric crater with inner crater and square outline faintly visible. Blocky debris is rare and appears to be randomly distributed. Small superposed craters are numerous. (*D*) Highly modified concentric crater with a faint indication of a square shape. Large blocks are rare and no trace of inner crater remains. A large population of small superposed craters is evident.

strength differences in the target rocks become less significant in controlling the morphology developed.

Origin of Surface and Substrate Layers

Evidence has been offered that the craters considered in this study are of impact origin. It has also been demonstrated that the craters that penetrate the substrate produce additi fragmented debris that is added to the sur layer. It can also be shown that there is a lationship between the freshness of concen craters and the number of craters superpo on the surrounding debris aprons. This relati ship, shown in Figure 19, is most certainly a result of erosional processes. With time and

bombardment, t and more batte degrees of crate on the moon. C represent only t ters in a long events. If such long time, a sur would be present The distributi areas determined with such an ori on various scales

Fig. 20. Concer

bombardment, the fresh craters become more and more battered and less recognizable. All degrees of crater freshness can be recognized on the moon. Craters considered in this study represent only the most recently produced craters in a long continued sequence of impact events. If such a process has continued for a long time, a surface layer of fragmental debris should be present.

The distributions of thickness in different areas as determined in this study are compatible with such an origin. Similarity of distributions at various scales of examination are to be expected in deposits originating from impact comminution. Furthermore, the median thickness of the layer in areas studied appears to be related to the density of the crater population. For example, the median thickness in the Lunar Orbiter 2 P13 and Lunar Orbiter 3 P12 sites is in the 3- to 6-meter range. The terrain in each site is relatively smooth and the density of larger craters is not high. On the other hand, the median thickness calculated for the Lunar Orbiter 2 P7 site is in the 6- to 9-meter range. The terrain there is much rougher and the density of large craters appears to be much greater.

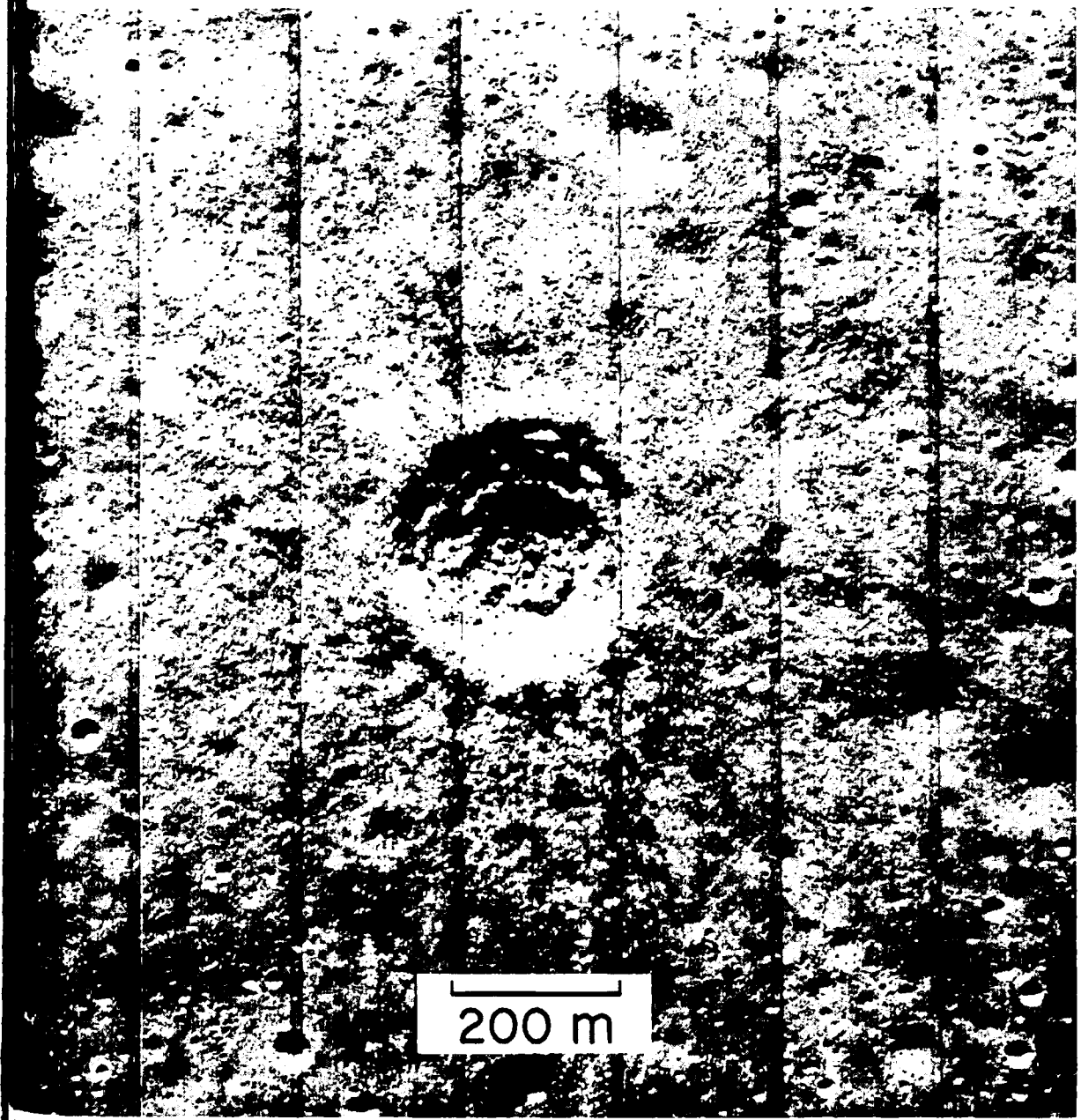

Fig. 20. Concentric crater with a multiplicity of nested central craters suggesting the presence of interbedded strata of varying strength in the substrate.

If this relationship holds for other areas, it would be strongly indicative of an impact origin for the surface layer.

The evidence presented above does not prove that the layer is exclusively of impact origin, but it does indicate that impact has contributed debris to the layer. Contributions from volcanic eruptions are also probable. The numerous domes and crater-chain-rille associations visible on lunar photographs indicate that the moon has had a volcanic history. The authors believe, however, that the extremely widespread but thin deposit of fragmental material on the lunar surface is more compatible with an impact comminution origin than it is with a volcanic origin. That is, the bulk of this debris in any one place was produced by randomly distributed local processes and has not been transported great distances from centers of volcanic activity.

The hard rocks that make up the substrate, on the other hand, were most probably produced by volcanic flows as the last major products of a phase of lunar volcanic activity. It may be that an extensive sequence of volcanic rocks will be revealed by stratigraphic studies of the maria rocks. Indeed, the presence of a sequence of interlayered hard and fragmental strata is indicated by certain concentric craters that contain a multiplicity of nested central craters. An example of this morphologic type is illustrated in Figure 20. The several terrace levels exposed are thought to represent hard, flow layers separated by beds of fragmental debris, a sequence characteristic of many volcanic terrains on the earth.

Conclusion

The preponderance of the normal, central-mound, flat-bottomed, and concentric craters observed on the moon and discussed in this paper were almost certainly formed by the impact process. Extensive laboratory study of the mechanics of formation and effects of variables on the formation of impact craters having these morphologies has shown that the thickness of the lunar surface layer can be determined within narrow limits using laboratory data and the observed distributions of the various morphologic types of craters. Application of these techniques will make it possible to add the third dimension to selenologic studies. Limited application of these techniques has shown already that the surface layer is thicker in Sinus Medii than it is in two areas of Oceanus Procellarum and that layer thickness may correlate with cratering density and thus possibly with age of the substrates. Additional measurements of the thickness of the surface layer in many regions of the moon will provide information required for interpretations of historical selenology.

References

Cherkasov, I. I., V. M. Vakhnin, A. L. Kemurjian, L. N. Mikhailov, V. V. Mikheyev, A. A. Musatov, M. J. Smorodinov, and V. V. Shvarev, Determination of physical and mechanical properties of the lunar surface layer by means of Luna 13 automatic station, Tenth Plenary Meeting, Cospar, London, 1967, in press, 1968.

Choate, R., Lunar slope angles and surface roughness from Ranger photographs, *Jet Propulsion Lab. Tech. Rept. 32-994*, Pasadena, Calif., 1968.

Christensen, E. M., S. A. Batterson, H. E. Benson, R. Choate, L. D. Jaffe, R. H. Jones, H. Y. Ko, R. L. Spencer, F. B. Sperling, and G. H. Sutton, Lunar surface mechanical properties, pp. 112–153, Surveyor III Mission Report, Part II, Scientific Results, *Jet Propulsion Lab. Tech. Rept. 32-1177*, Pasadena, Calif., 1967.

Gault, D. E., W. L. Quaide, and V. R. Oberbeck, Impact cratering mechanics and structures, *Proc. Conf. Shock Metamorphism of Natural Materials*, Goddard Space Flight Center, Greenbelt, Md., in press, 1968.

Gault, D. E., W. L. Quaide, V. R. Oberbeck, and H. J. Moore, Luna 9 photographs: Evidence for a fragmental surface layer, *Science*, 985–988, 1966.

Oberbeck, V. R., and W. L. Quaide, Estimated thickness of a fragmental surface layer of Oceanus Procellarum, *J. Geophys. Res.*, 4697–4704, 1967.

Rennilson, J. J., J. L. Dragg, E. C. Morris, E. M. Shoemaker, and A. Turkevich, Lunar surface topography, pp. 1–44, Surveyor I Mission Report, Part II, Scientific Results, *Jet Propulsion Lab. Tech. Rept. 32-1023*, Pasadena, Calif., 1966.

Scott, R. F., and F. I. Roberson, Soil mechanics surface samples: Lunar surface tests, results, analyses, pp. 69–110, Surveyor III Mission Report, Part II, Scientific Results, *Jet Propulsion Lab. Tech. Rept. 32-1177*, Pasadena, Calif., 1967.

Shoemaker, E. M., R. M. Batson, H. E. Holt, E. C. Morris, J. J. Rennilson, and E. A. Whitaker, Television observations for Surveyor III, pp. 9–67, Surveyor III Mission Report, Part II, Scientific Results, *Jet Propulsion Lab. Tech. Rept. 32-1177*, Pasadena, Calif., 1967.

(Received February 23, 1968; revised May 9, 1968.)